Blood First Edition Paper, prepublished online August 3, 2017; DOI 10.1182/blood-2016-11-754382

The actin binding protein profilin 2 is a novel regulator of iron homeostasis

Sara Luscieti[1,2], Bruno Galy[3], Lucia Gutierrez[4,5], Michael Reinke[6], Jorge Couso[1,2], Maya Shvartsman[1,7], Antonio Di Pascale[8], Walter Witke[6], Matthias W. Hentze[9], Pietro Pilo Boyl[6], Mayka Sanchez[1,2]

[1] Program of Predictive and Personalized Medicine of Cancer, Germans Trias and Pujol Research Institute (PMPPC-IGTP), Campus Can Ruti, Badalona, Spain

[2] Iron metabolism: regulation and diseases group, Josep Carreras Leukaemia Research Institute (IJC), Campus ICO - Germans Trias i Pujol, Badalona, Spain

[3] Division of Virus-associated Carcinogenesis, German Cancer Research Centre (DKFZ), Heidelberg, Germany

[4] Department of Biomaterials and Bioinspired Materials, Instituto de Ciencia de Materiales de Madrid (ICMM-CSIC), Madrid, Spain

[5] Current address: Analytical Chemistry Department, Institute of Nanoscience of Aragon (INA), Universidad de Zaragoza, Zaragoza, Spain

[6] Institute of Genetics, University of Bonn, Bonn, Germany

[7] Current address: European Molecular Biology Laboratory (EMBL), Monterotondo, Italy

[8] Department of Pharmacy, University of Naples Federico II, Naples, Italy

[9] European Molecular Biology Laboratory (EMBL), Heidelberg, Germany

Key words: Profilin2, iron metabolism, Iron regulatory proteins

Corresponding authors: Mayka Sanchez msanchez@carrerasresearch.org and Pietro Pilo Boyl pietro.piloboyl@uni-bonn.de

Word count abstract: 202

ABSTRACT

Cellular iron homeostasis is controlled by the iron regulatory proteins (IRPs) 1 and 2 that bind cis-regulatory iron-responsive elements (IRE) on target mRNAs. We identified the profilin2 (Pfn2) mRNA, which encodes an actin binding protein involved in endocytosis and neurotransmitters release, as a novel IRP-interacting transcript and studied its role in iron metabolism. Combination of EMSA experiments and bioinformatic analyses led to the identification of an atypical and conserved IRE in the 3' untranslated region of *Pfn2* mRNA. *Pfn2* mRNA levels were significantly reduced in duodenal samples from mice with intestinal-IRP ablation, suggesting that IRPs exert a positive effect on *Pfn2* mRNA expression *in vivo*. Over-expression of Pfn2 in HeLa and Hepa1-6 cells reduced their metabolically active iron pool. Importantly, Pfn2-deficient mice showed iron accumulation in discrete areas of the brain (olfactory bulb, hippocampus and midbrain) and reduction of the hepatic iron store without anaemia. In spite of low liver iron levels, hepatic hepcidin expression remained high, likely due to compensatory activation of *Hepcidin* by mild inflammation. Splenic ferroportin was increased probably to sustain hematopoiesis. Overall, our results indicate that Pfn2 expression is controlled by the IRPs *in vivo* and that Pfn2 contributes to maintaining iron homeostasis in cell lines and mice.

Key Points

- *Pfn2* mRNA has a functional and conserved 3' UTR Iron-Responsive Element (IRE).
- Pfn2 knock-out mice display an iron phenotype with iron accumulation in specific areas of the brain and depletion of liver iron stores.

Word count: 4250 words

Introduction

Cellular iron metabolism is maintained post−transcriptionally by iron regulatory proteins (IRP) 1 and 2, which bind conserved RNA stem-loop structures named iron−responsive element (IRE).[1] IRPs bind to IREs present in mRNAs that encode proteins involved in iron acquisition [transferrin receptor 1, Tfr1, a.k.a. *Tfrc*; divalent metal transporter 1, Dmt1, a.k.a. *Slc11a2*], storage [ferritin H, Fth1*;* ferritin L, Ftl], utilization [erythroid 5-aminolevulinic acid synthase, Alas2; mitochondrial aconitase, Aco2], export [ferroportin, Fpn a.k.a. *Slc40a1*] and iron/oxygen sensing [hypoxia-inducible factor 2-alpha, Hif2a, a.k.a. *EPAS1*].[2-5]

Functional IREs present a small asymmetrical cytosine bulge on the 5' strand of the stem and a 6-nucleotide apical loop with the sequence 5'-CAGWGH-3' (W =adenosine or uridine and H =adenosine, cytosine or uridine). The first cytosine and the fifth guanosine are pairing, forming an AGW pseudotriloop. The IRP1-IRE crystal structure revealed that the C-bulge and the pseudotriloop residues are important protein contact points.[6] The IRE upper stem consists of five paired nucleotides with or without the presence of an extra unpaired uridine residue downstream the apical loop (*Slc11a2* and *Epas1* IREs), while the lower stem is of variable length.[7-8]

IRP binding to IREs is regulated by intracellular iron levels as well as by nitric oxide, oxidative stress, and hypoxia. IRP activity is high in iron-deficient cells and low in iron-replete conditions. Both IRPs inhibit translation when bound to an IRE located in the 5' untranslated region (UTR), whereas their association with *Tfrc* 3' UTR IREs prevents mRNA degradation.[7-9]

Combined, body-wide ablation of both IRP1 and 2 in mice is embryonically lethal, showing that the IRP/IRE system is essential.[10-11] Tissue specific co-ablation of both proteins also revealed important functions of the IRPs in the intestine[12-13], the liver[14] as well as in

macrophage-mediated immunity. [15] On the other hand, excessive accumulation of IRP2 seemed lethal in mice[16], while a moderate gain of IRP1 function due to expression of a constitutively active *Irp1* transgene resulted in macrocytic erythropenia associated with impaired erythroid differentiation.[17]A key, yet unresolved question is whether all biological functions of IRP1 and/or IRP2 are achieved through regulation of the currently known IRE-containing genes, or whether there are other targets. We recently determined the IRP/IRE regulatory repertoire on a transcriptome-wide scale and identified novel mRNAs that bind to both IRPs,[18] including *profilin 2* (*Pfn2*).

Profilins constitute a family of small monomeric actin-binding proteins containing an actin-binding domain, a poly-L-proline binding domain and a phosphatidylinositol bisphosphate binding domain.[19] In mammals, four different profilin genes have been identified (*Pfn1*, *Pfn2*, *Pfn3* and *Pfn4)* with Pfn2 being predominantly expressed in the central nervous system. In mouse brain Pfn2 interacts with vesicle and membrane trafficking proteins such as dynamin1 (Dnm1), a multimeric GTPase required for receptor-mediated endocytosis.[20-21] Pfn2 binds with high affinity to Dnm1, resulting in its sequestration and thereby inhibiting endocytosis in neurons.[22-23] Pfn2 ablation in mice results in viable rodents born with the expected Mendelian ratio, although about 20% of the mutant pups do not reach weaning age, possibly due to behavioral deficits (PPB, unpublished observations). Compared to control, Pfn2-null animals are hyper-reactive and show increased locomotion and exploratory behavior. This phenotype correlates with increased synaptic excitability and higher neurotransmitter vesicle exocytosis in glutamatergic neurons of the cortico-striatal pathway, due to high probability of synaptic vesicle release;[24] therefore, Pfn2 appears to also negatively regulate vesicle exocytosis.[24]

In this work, we report the identification of a conserved IRE in the 3' UTR of the *Pfn2* mRNA, and provide evidence that Pfn2 expression is modulated *in vivo* by the IRPs. We show that Pfn2 knock-out mice have a hitherto unnoticed iron phenotype, with

accumulation of the metal in specific areas of the brain and a concomitant depletion of liver iron stores. This study uncovers a novel player in the IRP/IRE regulatory system and unveils the previously unrecognized importance of Pfn2 for iron homeostasis.

Methods

Animals

Mice were kept on a constant 12 hours light/dark cycle and food and water were supplied *ad libitum*. Male wild-type and *Pfn2*$^{-/-}$ littermates[24] on a C57Bl6/J genetic background were sacrificed at 7-9 months of age by cervical dislocation and dissected tissues were flash-frozen in liquid nitrogen for RNA, protein, and iron quantification studies. For histological analysis, mice were anesthetized with Ketamin and Xylazin (respectively 1 mg and 0.1 mg per 10 g of body weight, i.p.) (Sigma-Aldrich) and subjected to transcardial perfusion. For hematological and biochemical studies, heparinized or EDTA blood was collected from tail vein or via cheek-bleeding. Bone marrow was flushed out from femur and tibia bones. All experiments were performed according to EU regulations (Licenses n. 19/2005-B and AZ 84-02.04.2013.A233).

Cell culture

HeLa and Hepa1-6 cells lines were obtained from ATCC (Wesel, Germany). Culture and transfection conditions for all cells used in the study are described in the supplemental data, available on the *Blood* website.

Plasmid construction

Plasmids (I-12.CATwt and mut) for the synthesis of human *FTH1*-IRE probes for EMSA were previously described.[25] Mouse and human *Pfn2* IRE sequences (wild type or ΔA mutated) were subcloned into the I-12.CAT plasmid by replacement of the wt *FTH1*-IRE sequence using annealed synthetic oligonucleotides. A mouse *Pfn2* full length cDNA clone was purchased from OriGene Technologies. Fragments A-E in *Pfn2* 3'UTR were amplified by PCR and cloned into pCMV-XL5 (OriGene Technologies) using EcoRI and HindIII restriction sites. The mutated fragment A was obtained by site-directed mutagenesis (Stratagene). Pfn2-Mut S138D plasmid was previously described[23]. Primers used for cloning are listed in supplemental table 1.

Non-radioactive competitive electrophoretic mobility shift assay (EMSA)

Competitive EMSAs were performed as previously described.[3,26-28] See supplemental data, available on the *Blood* website for further details.

RNA

Protocols for isolation of total RNA, reverse transcription, and quantitative polymerase chain reaction (qPCR) were described previously.[18,26] Expression levels of housekeeping mRNAs (*RPL19*, *Tbp* and *β-actin*) were used as calibration controls. Sequences for qPCR primers are listed in supplemental table 1.

Labile iron pool (LIP) assay and reactive oxygen species (ROS) detection

The cytosolic labile iron pool and ROS levels were measured by the fluorescent Calcein-AM method and the dichlorofluorescein assay, respectively, as previously described.[29,30] Details for both assays are provided in the supplemental data, available on the *Blood* website.

Plasma IL6 cytokine analysis

Whole blood was collected in EDTA tubes and centrifuged at 1,500 g for 15 min at 4 C. Plasma supernatants were aliquoted and frozen in liquid nitrogen. Plasma samples were diluted 1:2 in assay buffer and measured using the Mouse Angiogenesis/Growth Factor Magnetic Bead Kit for detection of IL6 (EMD Millipore; MAGPMAG-24K) together with xMAP platform (EMD Millipore) according to the manufacturer's instructions. The data was analyzed with the MILLIPLEX Analyst Software.

Tissue iron content

Liver, duodenum, spleen, kidney, lung, heart and skeletal muscle non-heme iron content was measured using the previously described bathophenanthroline colorimetric method.[31-32] Total iron content of brain areas and bone marrow was determined by atomic absorption

spectrometry as previously described.[33] Further details are described in the supplemental data, available on the *Blood* website.

Perls Prussian non-heme iron histochemistry

9-11 months old mice were used for histological staining of non-heme iron using the perfusion Perls method with 3,3'-diaminobenzidine(DAB) intensification as described.[34-35] A detailed protocol can be found in supplemental data, available on the *Blood* website.

Total protein extraction and immunoblotting

Mouse tissues were lysed on ice in 44 mM Tris/HCl pH 6.8, 8% glycerol, 1.5% SDS, 3.2% b-mercaptoethanol, 0.12% w/v BPB using a glass Teflon douncer homogenizer at 600 rpm. Samples were then incubated for 10 min at 99°C (for ferroportin detection, the heat denaturation step was omitted). Total protein concentration was determined using the Pierce BCA Protein Assay kit (Themo Scientific) or the BioRad Bradford reagent following the manufacturer's instructions. For details, see supplemental data available on the *Blood* website.

Statistics

Data are shown as mean values ± SEM unless otherwise indicated. Statistical analysis was performed using two-tailed Student's t-test if two groups were compared, or one-way ANOVA test with Bonferroni multiple comparison test if three or more groups were compared. P-values are reported as follows:* $0.01<P$ value≤ 0.05, ** $0.001<P$ value≤ 0.01, *** P value≤ 0.001. Statistical analysis of Affymetrix microarrays was performed using a moderated Student's t-test with Linear Models for Microarray Data (LIMMA)[36] and P-value adjusted for multiple comparisons with FDR.[37]

See supplemental data, available on the *Blood* website for details of microarray analysis, Transmission Electron Microscopy (TEM) and Energy Dispersive X-ray Spectroscopy (EDS) measurements.

Results

Identification of *Pfn2* as a novel IRP binding mRNA with a conserved 3' UTR IRE

We have previously identified novel mRNAs that interact with IRP1 and/or IRP2 by combining immunoprecipitation and microarray analysis.[18,38] Three independent Affymetrix probes identified *Pfn2* as a mRNA associated with both IRPs in several mouse tissues. Although bioinformatics predictive tools such as the SIREs algorithm[39] fail to recognize a canonical IRE motifs in the *Pfn2* transcript, the *Pfn2* mRNA was enriched in a pull-down assay using recombinant IRP1 and RNA extracted from mouse spleen, brain, or liver (2.4 to 11.4 fold enrichment of *Pfn2* mRNA, depending on tissue) (Supplemental Figure 1). Furthermore, a full length *Pfn2* transcript could displace the interaction between recombinant IRP1 and a ferritin H IRE probe in a competitive EMSA, while a *Pfn2* transcript with most of its 3'UTR deleted could not (Figure 1C). These results indicate that the *Pfn2* mRNA interacts with IRP1 through an element located within its 3'UTR.[18]

To delineate the exact position of this element, we subcloned and tested 5 overlapping 250bp fragments of the *Pfn2* mRNA 3' UTR (Figure 1A) in competitive EMSAs using recombinant IRP1 (Figure 1C) or IRP2 (Supplemental Figure 3A). We found that the interaction between the *Pfn2* mRNA and the IRPs was mediated by the most upstream region (fragment A) of the *Pfn2* mRNA 3'UTR (Figure 1C and supplemental Figure 3). A detailed mRNA folding analysis identified a non-canonical IRE motif 326 bp downstream the stop codon (Figure 1B). The *Pfn2* IRE motif is conserved across several mammalian species (Figure 1E and supplemental Figure 2) and similarly to other IREs, it consists of a 5-paired upper stem and a mid-stem C bulge (C8) (Figure 1B), but differs from a canonical motif by the sequence of the hexanucleotide apical loop (**A**AGU**U**G instead of **C**AGU**G**H). Nonetheless, the first and the fifth ribonucleotide (adenosine and uridine) can pair, allowing the formation of an AGU pseudotriloop (Figure 1B), and deletion of the first adenosine in the apical loop (**A**AGUUG, Figure 1B) of the mouse and human *PFN2* IREs

abrogates binding to IRP1 and IRP2, as assessed by competitive EMSA (Figure 1D and Supplemental Figure 3A). We also demonstrated that the IRP-IRE competitive binding is dose-dependent for *Pfn2* mRNA (supplemental Figure 3B). Of note, two isoforms of the mouse *Pfn2* mRNA have been described[40]. These splice variants differ in the first 267bp of the last exon and yield two proteins with different C-terminal amino-acid composition[40-41], but both retain the 3'-IRE motif.

Altogether, these results reveal the presence of a conserved IRE in the 3'UTR of *Pfn2* mRNA bound both by IRP1 and IRP2.

Modulation of Pfn2 expression by IRPs

The *Tfrc* mRNA, which contains five IREs in its 3'UTR, is stabilized upon IRP binding in iron deficient cells, and is conversely degraded in iron replete conditions when IRP activity is low. We therefore tested whether *Pfn2* mRNA expression is regulated by iron in 4 different cell lines (NIH3T3, RAW264, Hepa1-6 and AML12). Contrasting with *Tfrc*, *Pfn2* transcript levels did not increase upon iron chelation with DFO, as assessed by qPCR; we even observed a significant reduction of *Pfn2* mRNA levels in Hepa1-6 cells (supplemental Figure 4A-*Pfn2*). *Pfn2* mRNA expression was nonetheless reduced in Hepa1-6 cells upon iron loading with hemin (supplemental Figure 4A-*Pfn2*). A time course experiment in Hepa1-6 cell lines showed that *Pfn2* mRNA levels were significantly and constantly decreased after 5, 10, 15 and 20 hours of hemin treatment, similarly to the *Tfrc* mRNA, while *Pfn2* mRNA reduction after DFO treatment was only transient (supplemental Figure 4B). Because IRE activity can be context dependent[12] and the regulation of *Pfn2* via its 3'UTR IRE may not be recapitulated in cultured cell lines, we also tested if *Pfn2* mRNA expression was modulated in C57BL6 mice fed with a low iron diet. *Tfrc* mRNA expression was expectedly increased in the liver, duodenum and spleen of iron-deficient mice, but *Pfn2* mRNA remained unchanged (supplemental Figure 5). Hence, iron depletion alone

seems not to suffice to stimulate *Pfn2* mRNA expression neither in cultured cells nor in mice, at least under the experimental conditions tested.

We therefore took advantage of a mouse model with acute loss of IRP1 and IRP2 function in the intestinal mucosa to study the impact of the IRPs on *Pfn2* expression in vivo.[12] As expected, *Tfrc* mRNA levels were reduced by about 50 % (Figure 2). Importantly, *Pfn2* mRNA levels were also significantly decreased (25%). These results thus indicate that IRPs exert a positive effect on *Pfn2* mRNA expression, as expected for a 3' IRE-containing transcript.

Pfn2 reduces the labile iron pool of the cell.

Because *Pfn2* is regulated by the IRPs, the key regulators of iron metabolism in the cell, we next studied the influence of Pfn2 on cellular iron metabolism. Ectopic over-expression of wild type Pfn2 in HeLa cells was previously reported to inhibit endocytosis, thereby blocking transferrin uptake. This effect was not observed with a mutant Pfn2 form (Pfn2-Mut S138D) that binds actin but not dynamin 1[23].

To further study the effect of Pfn2 on cellular iron levels, we transiently over-expressed either a wild-type (wt) or a mutated (mut S138D) form of Pfn2 in HeLa cells and measured the iron labile pool (LIP). Over-expression of both clones was at similar levels (data not shown). As control, cells were either transfected with mouse H-ferritin (*Fth1*) or treated with DFO to chelate iron and thus reduce the LIP; conversely, they were treated with FAC to increase the LIP.

We found that overexpression of wt Pfn2 reduced the LIP as efficiently as Fth1 or DFO treatment, while over-expression of the S138D Pfn2 mutant had no effect (Figure 3A). Similar results were obtained in HeLa and Hepa1-6 cells stably over-expressing Pfn2 versus Pfn2-Mut S138D (Figure 3B). To further demonstrate that Pfn2 reduces cellular iron availability, we measured ROS levels in H_2O_2-treated cells. We found that transient wt Pfn2 expression reduced ROS levels in H_2O_2-treated HeLa cells, and that over-expression

of Pfn2-Mut S138D has no effect on ROS (Figure 3C). These data demonstrate that Pfn2 decreases the metabolically active iron pool in the cell.

Abnormal iron distribution in Pfn2-deficient mice

Pfn2$^{-/-}$ mice have been reported to have neuronal hyper-excitability due to increased synaptic vesicle exocytosis.[24] However, the role of Pfn2 in iron metabolism has not been addressed. In light of our finding that Pfn2 influences iron metabolism in cultured cells, we next studied the role of Pfn2 in iron metabolism *in vivo* in Pfn2-null mice.

Enhanced Prussian Blue staining of iron with the Perls perfusion method was performed in key organs of iron homeostasis including the duodenum (site of iron absorption), the liver (site of iron storage), the spleen (site of iron recycling), and the bone marrow (site of iron utilization). We also analyzed the brain and kidney due to high Pfn2 expression in those tissues. We did not observe any change in the amount and distribution of iron in the duodenum, spleen, bone marrow and kidney of Pfn2-deficient mice (data not shown). This was confirmed by quantification of total non-heme iron levels in duodenum, spleen and kidney with the bathophenanthroline chromogen method (Figure 4C), and by atomic absorption spectrometry measurement of total iron in bone-marrow (Figure 4D). Hence, Pfn2 seems dispensable for maintaining iron homeostasis in the intestine, spleen, kidney and bone-marrow of mice kept under standard laboratory conditions. Interestingly, iron deposits were observed in particular brain areas such as the Ammon's Horn of the hippocampus (Figure 4A). The analysis of dissected brain tissue by atomic absorption spectrometry confirmed the accumulation of iron in the hippocampus but also in the olfactory bulb and the midbrain of *Pfn2*$^{-/-}$ mice (Figure 4E). Contrasting with iron loading of neurons, liver parenchymal cells show a loss of iron stores (Figure 4B) and iron levels in the liver of Pfn2-null animals were reduced by 40% (Figure 4C). Similar results were obtained in 2-3 weeks old mice (data not shown), indicating that liver iron depletion occurs early in life. Depletion of the liver iron store was not due to increased urinary iron excretion

(Supplemental Figure 6) and was not associated with any hematological abnormality nor with any alteration of serum iron parameters (Supplemental Table 2).

Together, these results show that Pfn2 plays an important role in brain and liver iron metabolism.

Brain iron accumulation in *Pfn2*$^{-/-}$ mice

Total iron was selectively increased in the olfactory bulb, hippocampus and midbrain of 7-9 month-old *Pfn2*$^{-/-}$ mice, the three areas where Pfn2 expression levels are highest (Liemersdorf *et al*. manuscript in preparation), but was unchanged in other brain regions such as striatum, cortex and cerebellum (Figure 4E).

In spite of iron loading, ferritin protein levels in hippocampus were reduced (Figure 5A), with no concomitant change in *Fth1* and *Ftl* mRNA levels (Figure 5B). Transmission electron microscopy (TEM) in the hippocampus of *Pfn2*-deficient mice revealed abnormal electron-dense aggregates inside a subset of membrane organelles that resemble mitochondria, as indicated by the presence of lamellae (Figure 5C, white arrow). The presence of iron aggregates in hippocampus was confirmed by Energy Dispersive X-ray Spectroscopy (Figure 5D). A closer look at these organelles revealed two electron dense structures possibly corresponding to iron deposits: large amorphous biomineral aggregates (Figure 5C, arrow 1) and more defined nanoparticles (Figure 5C, arrow 2). Both entities are different from the typical iron aggregate present in spleen as ferritin shells (Figure 5C, arrow 3) or as hemosiderin (Figure 5C, arrow 4). Structurally, both hippocampal iron-containing species (arrow 1 and 2) differ from normal and pathological (observed in neurodegenerative diseases) cytoplasmic ferritins deposits[40, 42] and from the mitochondrial biomineral iron aggregates found in the heart of Friedreich ataxia mice [43].

Hepatic iron metabolism in *Pfn2*$^{-/-}$ mice

The decrease of liver iron content in *Pfn2*$^{-/-}$ mice was accompanied by a significant reduction of Ferritin L expression both at the protein (Figure 6A) and mRNA level (Figure

6C). In line with the decreased hepatic iron content, *Bmp6* mRNA expression in *Pfn2*$^{-/-}$ livers was reduced by 30% (Figure 6C). While the reduction of the liver iron content and the concomitant suppression of *Bmp6* would predict a decrease in hepcidin expression, hepatic *Hamp1* mRNA levels remain unchanged in *Pfn2*$^{-/-}$ mice (Figure 6C). We hypothesized that antagonistic cues such as inflammation [44] could counteract the regulation of *Hamp1* by low iron in *Pfn2*$^{-/-}$ animals. Indeed, expression array analysis of *Pfn2*$^{-/-}$ livers (Supplemental Table 3) revealed a mild activation of the IL6 pathway (activation Z-score: 0,247) associated with the up-regulation of several IL6-target genes (Supplementary Table 4). In line with this observation, plasma IL6 concentration was found to be elevated in *Pfn2*$^{-/-}$ animals (Figure 6B). Furthermore, *Pfn2*-deficient mice displayed a tendency for increased expression of several pro-inflammatory cytokine mRNAs in the liver, including *Saa1*, *Tnfα*, *ActivinB*, *Il1β* and *Il6* (Figure 6C). Thus, the failure to downregulate Hamp1 in Pfn2-/- animals with low hepatic iron stores could be explained by concomitant stimulation of the gene transcription under mild pro-inflammatory conditions.

Our expression array analysis overall showed 20 up-regulated and 29 down-regulated genes in the liver of *Pfn2*$^{-/-}$ mice compared to control littermates (representing 0.06% and 0.08%, respectively, of the tested transcriptome) (Supplemental Table 4). *Lipocalin2* (*Lcn2*), an iron-trafficking protein that mediates the uptake of siderophores and catechol-Fe(III) complexes, [45,46] was among the up-regulated genes and its increase was confirmed by qPCR (Figure 6C).

Iron uptake in liver is also dependent on Dmt1, which is encoded by the *Slc11a2* gene.[1] We analyzed the expression of the *Slc11a2*-IRE and non-IRE mRNA isoforms[47] by qPCR. We observed a statistically significant and specific up-regulation of the *Slc11a2*-IRE mRNA isoform in *Pfn2*$^{-/-}$ liver samples (Figure 6C), which could possibly be due to increased IRP binding to the *Slc11a2*-IRE mRNA under iron deficient conditions.

Spleen iron metabolism in *Pfn2*$^{-/-}$ mice

Spleen non-heme iron content and size was comparable between *Pfn2*$^{-/-}$ mice and control mice (Figure 4C and Supplemental Figure 7A). No evidence of extramedullary hematopoiesis was detected in *Pfn2*$^{-/-}$ mice (Supplemental Figure 7B and 7C). Splenic structural iron deposits studied by TEM were expectedly present in lysosome-like structures arranged in ≈5nm large electron-dense nanoparticles (corresponding to the ferritin iron core) that are usually described as hemosiderin (Figure 5C arrow 4). Accordingly, ferritin L and H mRNA and protein levels were not changed (Figure 6E and data not shown). However, we detected a statistically significant increase in ferroportin protein and RNA level in the spleen of *Pfn2*$^{-/-}$ mice (Figure 6D and E), which could serve as a mean to counter-balance the effect of inappropriately normal hepcidin levels on ferroportin membrane expression.

Discussion

IRP-mutant mouse models revealed that the IRP/IRE regulatory system is critical for securing physiological iron distribution between major sites of systemic iron homeostasis. Here, we describe a new IRP mRNA target, *Pfn2*, and unveil a novel function for this actin-binding protein in iron metabolism.

We show that *Pfn2* mRNA harbors a conserved and functional IRE in its 3' UTR. Similar to the well-characterized 3'IRE-containing *Tfrc* mRNA, *Pfn2* transcript levels are reduced upon IRP ablation *in vivo* in mice. Yet, steady-state *Pfn2* mRNA levels are largely unchanged under iron deficient conditions, both in cultured cells and in mice. The lack of iron regulation of *Pfn2* is not totally surprising, as it is already known that for example the modulation of the *Slc11a2* mRNA by iron is cell-line specific and is influenced by the differentiation state of the cell.[4] In addition, multiple integrative and opposing signals contribute to the regulation of several single IRE-containing mRNAs such as *Epas1* (protein HIF2alpha), *Slc40a1* (protein ferroportin) and *Slc11a2* (protein Dmt1). Overall, it seems that a straightforward regulation of 3' IRE-containing mRNAs by iron levels and

IRPs is only consistently observed in the case of *Tfrc*, although even for this transcript the fold regulation is very variable and depends on the cell line or tissue analyzed.

On the other hand, mice with constitutive deficiency of Pfn2 exhibit a striking iron phenotype, with iron accumulation in specific areas of the brain and a reduction of the liver iron stores, although displaying normal red blood cell counts and plasma iron parameters.

Iron accumulation in the brain of *Pfn2*$^{-/-}$ mice correlates with the expression pattern of Pfn2, being the highest in hippocampus, olfactory bulb and midbrain (Liemersdorf *et al.* manuscript in preparation). It is well established that iron bound to transferrin is internalized through receptor-mediated endocytosis of Tfr1, involving clathrin-coated pits and Dnm1.[48] Pfn2 interacts with and sequesters Dnm1 in neurons, thereby preventing its binding to endocytic effectors.[23] Thus, Pfn2 acts as a negative regulator of endocytosis. Indeed, neurons from Pfn2-knockout mice show increased endocytic rate and ectopic over-expression of Pfn2 in HeLa cells slows down transferrin uptake.[23] In this work, we observed that Pfn2 over-expression in several cell lines decreased the cLIP. Hence, it is conceivable that the iron overload in the brain of *Pfn2*$^{-/-}$ mice is due to an increased rate of transferrin-Tfr1 endocytosis in the absence of Pfn2 (Figure 7). Interestingly, we show that iron accumulation in hippocampus of *Pfn2*$^{-/-}$ mice occurs in previously undescribed biomineral iron forms inside organelles whose membrane structure resembles mitochondria. As *Pfn2*$^{-/-}$ mice do not manifest overt neurodegeneration or ataxia, we hypothesize that the iron aggregates could be a harmless way to confine the otherwise highly toxic iron excess inside the neurons.

While iron accumulates in the brain of *Pfn2*$^{-/-}$ mice, we were surprised to observe a substantial depletion of the liver iron stores. Although microarray data did not reveal major alterations in this tissue, we observed up-regulation of genes involved in liver uptake of extracellular iron that could likely be a compensatory mechanism to reestablish hepatic iron stores. The liver iron content of Pfn2-null mice is deficient in the context of unchanged

spleen and duodenal iron levels as well as normal red blood cell counts and serum iron parameters. Hence, it cannot be explained by the classical mobilization of the hepatic iron stores in conditions of anemia. Future work is needed to elucidate this phenomenon.

Our hepatic expression analysis revealed one contradictory situation in low iron stores condition: *Bmp6* levels were low, while *Hamp1* transcript levels were not decreased. Our microarray and qPCR data in liver and our plasma IL6 measurements indicate a mild chronic systemic inflammation in *Pfn2*$^{-/-}$ mice. As the absence of Pfn2 is known to increase neurotransmitter release,[24] it is possible that it affects similarly the release of cytokines produced in different tissues. Therefore, the observed reduction in hepatic *Bmp6* mRNA expression and the increased levels of IL6 may act as antagonistic signals, maintaining an overall stable *Hamp1* expression.

Spleen non-heme iron content and size was found unchanged in *Pfn2*$^{-/-}$ mice. Nevertheless, ferroportin expression was increased in spleens of *Pfn2*$^{-/-}$ mice. Since hepcidin negatively regulates membrane ferroportin levels, it is conceivable that increased ferroportin expression in spleen serves to stabilize its membrane presence in order to compensate hepatic iron deficiencies and sustain hematopoiesis, as Pfn2$^{-/-}$mice are not anemic (Figure 7).

Our work highlights that altering the expression of a key regulator of membrane trafficking and endocytosis pathways such as Pfn2 alters iron metabolism at the cellular level and affects body iron homeostasis, similarly to defects in other endosomal sorting proteins such as Snx3[49], or Sec15l1[50]. In summary, our studies indicate that Pfn2 is a previously unrecognized critical player in iron homeostasis, which could contribute to human disorders of iron metabolism.

Acknowledgements

We thank Dunja Ferring-Appel for excellent technical assistance with serum iron parameter measurements and Anke Carstensen from the Institut für Klinische Chemie und Klinische Pharmakologie –Zentrallabor- Ltd. MTA, Universitätsklinikum Bonn for performing the blood analyses on the mice. Dr. Lara Nonell from the Microarray Analysis Service of the Hospital del Mar Medical Research Institute (IMIM) for support with microarray analysis. Dr. Mar Mallo and Dr. Francesc Sole from the Affymetrix Microarray Platform of the Josep Carreras Leukaemia Research Institute (IJC-PAM) for microarray performance. Authors acknowledge the facilities and the scientific and technical assistance of Cristina Patiño, Rocío San Andrés and Javier Bueno, from the TEM service at CNB and Dr. M. Puerto Morales from Instituto de Ciencia de Materiales de Madrid (ICMM-CSIC), Madrid, Spain for continuous support.

This work was supported by grant SAF2015-70412-R from Spanish Secretary of Research, Development and Innovation (MINECO) and grant DJCLS R14/04 from Deutsche José Carreras Leukämie Stiftung, grant 2014 SGR225 (GRE) from Generalitat de Catalunya and economical support from Fundació Internacional Josep Carreras and from Obra Social “la Caixa” Spain to M.S. All work on the Pfn2 knockout mouse model was supported by the Deutsche Forschungsgemeinschaft (DFG) SFB1089 grant.

Authorship

Contribution: M.S., P.B.P designed and performed research, analyzed the data, and wrote the manuscript. L.G., B.G., provided reagents and samples, analyzed the data and wrote the manuscript. M.W.H., W.W. provided reagents and analyzed the data. S.L., L.G., M.Sh., M.R., J.C., A.D.P. performed research and analyzed the data.

The authors declare no competing financial interests.

References

1. Hentze MW, Muckenthaler MU, Galy B, Camaschella C. Two to tango: regulation of Mammalian iron metabolism. *Cell*. 2010;142(1):24-38.
2. Anderson CP, Shen M, Eisenstein RS, Leibold EA. Mammalian iron metabolism and its control by iron regulatory proteins. *Biochim Biophys Acta*. 2012;1823(9):1468-1483.
3. Sanchez M, Galy B, Muckenthaler MU, Hentze MW. Iron-regulatory proteins limit hypoxia-inducible factor-2alpha expression in iron deficiency. *Nat Struct Mol Biol*. 2007;14(5):420-426.
4. Gunshin H, Allerson CR, Polycarpou-Schwarz M, et al. Iron-dependent regulation of the divalent metal ion transporter. *FEBS Lett*. 2001;509(2):309-316.
5. McKie AT, Marciani P, Rolfs A, et al. A novel duodenal iron-regulated transporter, IREG1, implicated in the basolateral transfer of iron to the circulation. *Mol Cell*. 2000;5(2):299-309.
6. Walden WE, Selezneva AI, Dupuy J, et al. Structure of dual function iron regulatory protein 1 complexed with ferritin IRE-RNA. *Science*. 2006;314(5807):1903-1908.
7. Wilkinson N, Pantopoulos K. The IRP/IRE system in vivo: insights from mouse models. *Front Pharmacol*. 2014;5:176.
8. Joshi RS ME, Sanchez M. Cellular Iron Metabolism – The IRP/IRE Regulatory Network. In: Arora S ed. Iron metabolism: InTech; 2012.
9. Yoshinaga M, Nakatsuka Y, Vandenbon A, et al. Regnase-1 Maintains Iron Homeostasis via the Degradation of Transferrin Receptor 1 and Prolyl-Hydroxylase-Domain-Containing Protein 3 mRNAs. *Cell Rep*. 2017;19(8):1614-1630.
10. Galy B, Ferring D, Hentze MW. Generation of conditional alleles of the murine Iron Regulatory Protein (IRP)-1 and -2 genes. *Genesis*. 2005;43(4):181-188.
11. Smith SR, Ghosh MC, Ollivierre-Wilson H, Hang Tong W, Rouault TA. Complete loss of iron regulatory proteins 1 and 2 prevents viability of murine zygotes beyond the blastocyst stage of embryonic development. *Blood Cells Mol Dis*. 2006;36(2):283-287.
12. Galy B, Ferring-Appel D, Becker C, et al. Iron regulatory proteins control a mucosal block to intestinal iron absorption. *Cell Rep*. 2013;3(3):844-857.
13. Galy B, Ferring-Appel D, Kaden S, Grone HJ, Hentze MW. Iron regulatory proteins are essential for intestinal function and control key iron absorption molecules in the duodenum. *Cell Metab*. 2008;7(1):79-85.
14. Galy B, Ferring-Appel D, Sauer SW, et al. Iron regulatory proteins secure mitochondrial iron sufficiency and function. *Cell Metab*. 2010;12(2):194-201.
15. Nairz M, Ferring-Appel D, Casarrubea D, et al. Iron Regulatory Proteins Mediate Host Resistance to Salmonella Infection. *Cell Host Microbe*. 2015;18(2):254-261.
16. Moroishi T, Nishiyama M, Takeda Y, Iwai K, Nakayama KI. The FBXL5-IRP2 axis is integral to control of iron metabolism in vivo. *Cell Metab*. 2011;14(3):339-351.
17. Casarrubea D, Viatte L, Hallas T, et al. Abnormal body iron distribution and erythropoiesis in a novel mouse model with inducible gain of iron regulatory protein (IRP)-1 function. *J Mol Med (Berl)*. 2013.
18. Sanchez M, Galy B, Schwanhaeusser B, et al. Iron regulatory protein-1 and -2: transcriptome-wide definition of binding mRNAs and shaping of the cellular proteome by iron regulatory proteins. *Blood*. 2011;118(22):e168-179.
19. Witke W. The role of profilin complexes in cell motility and other cellular processes. *Trends Cell Biol*. 2004;14(8):461-469.
20. Damke H, Binns DD, Ueda H, Schmid SL, Baba T. Dynamin GTPase domain mutants block endocytic vesicle formation at morphologically distinct stages. *Mol Biol Cell*. 2001;12(9):2578-2589.

21. Ferguson SM, Brasnjo G, Hayashi M, et al. A selective activity-dependent requirement for dynamin 1 in synaptic vesicle endocytosis. *Science*. 2007;316(5824):570-574.
22. Witke W, Podtelejnikov AV, Di Nardo A, et al. In mouse brain profilin I and profilin II associate with regulators of the endocytic pathway and actin assembly. *EMBO J*. 1998;17(4):967-976.
23. Gareus R, Di Nardo A, Rybin V, Witke W. Mouse profilin 2 regulates endocytosis and competes with SH3 ligand binding to dynamin 1. *J Biol Chem*. 2006;281(5):2803-2811.
24. Pilo Boyl P, Di Nardo A, Mulle C, et al. Profilin2 contributes to synaptic vesicle exocytosis, neuronal excitability, and novelty-seeking behavior. *EMBO J*. 2007;26(12):2991-3002.
25. Gray NK, Quick S, Goossen B, et al. Recombinant iron-regulatory factor functions as an iron-responsive-element-binding protein, a translational repressor and an aconitase. A functional assay for translational repression and direct demonstration of the iron switch. *Eur J Biochem*. 1993;218(2):657-667.
26. Sanchez M, Galy B, Dandekar T, et al. Iron regulation and the cell cycle: identification of an iron-responsive element in the 3'-untranslated region of human cell division cycle 14A mRNA by a refined microarray-based screening strategy. *J Biol Chem*. 2006;281(32):22865-22874.
27. Luscieti S, Tolle G, Aranda J, et al. Novel mutations in the ferritin-L iron-responsive element that only mildly impair IRP binding cause hereditary hyperferritinaemia cataract syndrome. *Orphanet J Rare Dis*. 2013;8:30.
28. Liu Z, Lanford R, Mueller S, et al. Siderophore-mediated iron trafficking in humans is regulated by iron. *J Mol Med (Berl)*. 2012.
29. Epsztejn S, Kakhlon O, Glickstein H, Breuer W, Cabantchik I. Fluorescence analysis of the labile iron pool of mammalian cells. *Anal Biochem*. 1997;248(1):31-40.
30. Santamaria R, Irace C, Festa M, Maffettone C, Colonna A. Induction of ferritin expression by oxalomalate. *Biochim Biophys Acta*. 2004;1691(2-3):151-159.
31. Torrance JD, Bothwell TH. A simple technique for measuring storage iron concentrations in formalinised liver samples. *S Afr J Med Sci*. 1968;33(1):9-11.
32. Patel BN, Dunn RJ, Jeong SY, Zhu Q, Julien JP, David S. Ceruloplasmin regulates iron levels in the CNS and prevents free radical injury. *J Neurosci*. 2002;22(15):6578-6586.
33. Gutierrez L, Quintana C, Patino C, et al. Iron speciation study in Hfe knockout mice tissues: magnetic and ultrastructural characterisation. *Biochim Biophys Acta*. 2009;1792(6):541-547.
34. Meguro R, Asano Y, Iwatsuki H, Shoumura K. Perfusion-Perls and -Turnbull methods supplemented by DAB intensification for nonheme iron histochemistry: demonstration of the superior sensitivity of the methods in the liver, spleen, and stomach of the rat. *Histochem Cell Biol*. 2003;120(1):73-82.
35. Rodrigues PN, Gomes SS, Neves JV, et al. Mycobacteria-induced anaemia revisited: a molecular approach reveals the involvement of NRAMP1 and lipocalin-2, but not of hepcidin. *Immunobiology*. 2011;216(10):1127-1134.
36. Smyth GK. Linear models and empirical bayes methods for assessing differential expression in microarray experiments. *Stat Appl Genet Mol Biol*. 2004;3:Article3.
37. Benjamini Y, Hochberg Y. Controlling the False Discovery Rate: A Practical and Powerful Approach to Multiple Testing. *Journal of the Royal Statistical Society*. 1995;57(1):289-300.
38. Sanchez M, Galy B, Hentze MW, Muckenthaler MU. Identification of target mRNAs of regulatory RNA-binding proteins using mRNP immunopurification and microarrays. *Nat Protoc*. 2007;2(8):2033-2042.

39. Campillos M, Cases I, Hentze MW, Sanchez M. SIREs: searching for iron-responsive elements. *Nucleic Acids Res*. 2010;38 Suppl:W360-367.
40. Di Nardo A, Gareus R, Kwiatkowski D, Witke W. Alternative splicing of the mouse profilin II gene generates functionally different profilin isoforms. *J Cell Sci*. 2000;113 Pt 21:3795-3803.
41. Lambrechts A, Braun A, Jonckheere V, et al. Profilin II is alternatively spliced, resulting in profilin isoforms that are differentially expressed and have distinct biochemical properties. *Mol Cell Biol*. 2000;20(21):8209-8219.
42. Quintana C, Gutierrez L. Could a dysfunction of ferritin be a determinant factor in the aetiology of some neurodegenerative diseases? *Biochim Biophys Acta*. 2010;1800(8):770-782.
43. Whitnall M, Suryo Rahmanto Y, Huang ML, et al. Identification of nonferritin mitochondrial iron deposits in a mouse model of Friedreich ataxia. *Proc Natl Acad Sci U S A*. 2012;109(50):20590-20595.
44. Nemeth E, Rivera S, Gabayan V, et al. IL-6 mediates hypoferremia of inflammation by inducing the synthesis of the iron regulatory hormone hepcidin. *J Clin Invest*. 2004;113(9):1271-1276.
45. Devireddy LR, Gazin C, Zhu X, Green MR. A cell-surface receptor for lipocalin 24p3 selectively mediates apoptosis and iron uptake. *Cell*. 2005;123(7):1293-1305.
46. Bao G, Clifton M, Hoette TM, et al. Iron traffics in circulation bound to a siderocalin (Ngal)-catechol complex. *Nat Chem Biol*. 2010;6(8):602-609.
47. Hubert N, Hentze MW. Previously uncharacterized isoforms of divalent metal transporter (DMT)-1: implications for regulation and cellular function. *Proc Natl Acad Sci U S A*. 2002;99(19):12345-12350.
48. van der Bliek AM, Redelmeier TE, Damke H, Tisdale EJ, Meyerowitz EM, Schmid SL. Mutations in human dynamin block an intermediate stage in coated vesicle formation. *J Cell Biol*. 1993;122(3):553-563.
49. Chen C, Garcia-Santos D, Ishikawa Y, et al. Snx3 regulates recycling of the transferrin receptor and iron assimilation. *Cell Metab*. 2013;17(3):343-352.
50. Lim JE, Jin O, Bennett C, et al. A mutation in Sec15l1 causes anemia in hemoglobin deficit (hbd) mice. *Nat Genet*. 2005;37(11):1270-1273.

Figure legends

Figure 1. Identification of the Pfn2 3' IRE and IRP binding studies. (A) Schematic representation of the *Pfn2* mRNA. Coding region (black box), *Pfn2* XcmI fragment and fragments A to E and IRE are shown. (B). Human and mouse 3' IRE motifs in *Pfn2*, *Tfrc* and *Slc11a2* mRNAs. Notice differences in sequence in the apical loop. The arrow indicates the deletion of the adenosine (ΔA, mut) used as mutant construct. (C) Non-radioactive competitive EMSA using fluorescent *Ferritin-H* IRE labeled probe and 2x fold molar excess of unlabeled competitors (full length *Pfn2* mRNA or *Pfn2* mRNA fragments). Constructs or fragments (XcmI fragment, A to E fragment) used as competitors are indicated. WT denotes wild-type fragment A and Mut denotes fragment A containing a single deletion in the first A of the 6-nucleotides apical loop. One representative experiment out of 4 is shown. (D) Non-radioactive competitive EMSA using fluorescent *Ferritin-H* IRE labeled probe and 80x fold molar excess of unlabeled competitors (*Ferritin H* or mouse and human *Pfn2* IRE sequences). (E) Representative phylogenic conservation of the *Pfn2* IRE among mammals, 100% conserved residues are indicated with an asterisk (*), an extended alignment is shown in supplemental figure 2.

Figure 2. Duodenal expression levels of Pfn2 in mice with intestinal IRP1 and IRP2 deficiency in adult stage. IRP1 and IRP2 deficiency was obtained using the CRE/Lox technology in a tamoxifen-inducible system in the intestinal mucosa. Adult animals carrying floxed IRP alleles plus the CRE transgene were given tamoxifen (1 mg i.p. per animal per day on 5 consecutive days) to trigger IRP ablation in the intestine. Mice were sacrificed 5 weeks after the last tamoxifen injection. Control mice (white bars) were wt mice treated with oil (no CRE oil) or tamoxifen (no CRE tamoxifen), or CRE-expressing mice receiving the vehicle only (CRE oil). *Tfrc* mRNA expression was assessed as a molecular signature of IRP deficiency. The histograms represent mRNA levels after

calibration to beta-actin and normalization to the “no Cre oil” control. P-values were determined by unpaired two-tailed Student’s t-test , **p<0.01,*** p<0.001.

Figure 3. Labile iron pool (LIP) and reactive oxygen species (ROS) levels in cell lines over-expressing Pfn2. (A) HeLa cells were transiently transfected with pCMV6-Kan/Neo empty vector, pCMV6-Pfn2 or Pfn2-Mut S138D vector. As control, cells were transfected with pCMV6-Fth1 vector or with the empty vector and treated with 200µM DFO or 200µM FAC for 16h. Cytoplasmic labile iron pool (LIP) was measured by the calcein-AM method 48h after transfection. Data were normalized to cells transfected with the empty vector, set as 100%. Means ± SD are shown. (B) Stable Hepa1-6 and HeLa clones over-expressing the wild type mouse Pfn2 or Pfn2-Mut S138D were isolated and LIP was measured and normalized to cells stably transfected with the pCMV6 empty vector, set as 100%. Means ± SD are shown. (C) Reactive oxygen species (ROS) levels were measured using the 2’,7’-dichlorofluorescin diacetate method in HeLa cells transiently transfected with pCMV6-Kan/Neo empty vector, pCMV6-Pfn2, Pfn2-Mut S138D or pCMV6-Fth1 vectors or in cells transfected with the empty vectors and treated with 200µM DFO for 16h. ROS levels were assayed 48h after transfection following a pre-treatment with 200 µM H_2O_2 to induce ROS generation. ROS quantifications were normalized to cells transfected with the empty vector and not treated with H_2O_2, set as 100%. Means ± SD are shown.

Figure 4. Abnormal iron distribution in Pfn2$^{-/-}$ versus wild-type mice. Enhanced Prussian Blue staining in brain (A) and liver (B) of Perls perfused Pfn2$^{-/-}$ and wt mice. In the *Pfn2*$^{-/-}$ brain section the arrows point to CA1-CA2 hippocampal regions, enriched in iron. In contrast, iron is lost in liver parenchymal cells. Scale is 100 µm in (A), and 200 µm in low magnification panels and 20 µm in the high magnification insets in (B). (C) Tissue non-heme iron content measured using the bathophenantroline chromogen method in the

indicated tissues shows a loss of 40% of iron in the liver of Pfn2$^{-/-}$ mice. Total iron content measured by atomic absorption method in bone marrow (D) and brain areas (E) shows iron overload in olfactory bulbs, hippocampus and midbrain of Pfn2$^{-/-}$ mice. Measures are given as percentage of control wild-type littermates. The sample size (n) is indicated. P-values were determined by unpaired two-tailed Student's t-test , *p<0.05,** p<0.01.

Figure 5. Ferritin L and H protein and mRNA levels and iron deposits in the hippocampus of Pfn2$^{-/-}$ mice. (A) Hippocampal L-ferritin (Ftl) and H-ferritin (Fth1) protein measured by Western blotting are reduced in Pfn2 KO mice compared to wt controls. Ribosomal protein S6 levels were used for calibration. Graphs represent quantified data normalized to the wt control (set as 100%). Sample size (n) is indicated. (B) Hippocampal L-ferritin (*Ftl*) and H-ferritin (*Fth1*) mRNA levels measured by qPCR show no difference between Pfn2$^{-/-}$ and wt control mice. mRNA expression was calibrated with *ribosomal protein L19 (RPL9)* and *TATA box binding protein* (*Tbp*) mRNA expression and normalized to wild type mice (set as 100%). Sample size (n) is indicated. (C) On the left side, transmission electron micrograph (TEM) sample image from the hippocampus of a Pfn2$^{-/-}$ mouse. The boxed area is magnified on its right. On the right side, sample image from the spleen of a Pfn2$^{-/-}$ mouse.TEM images of hippocampus (second image) and spleen (third image from left) are at the same magnification for comparison of the aggregates size and morphology. Lamellae structures characterizing a mitochondrion are highlighted by a white arrow. Iron aggregates of different morphology are indicated by yellow arrows: mitochondrial amorphous and big clustered aggregates (1), isolated biomineral nanoparticles (2), cytoplasm dispersed ferritin cores (3) and spleen hemosiderin aggregates (4). Small insets from center and right TEM images are at the same magnification, showing the smaller particle size observed in hippocampus (2) in comparison with the spleen ferritin cores (3). (D) In the hippocampus and spleen of Pfn2$^{-/-}$

mice, electron-dense areas have been tested by Energy Dispersive X-ray Spectroscopy (EDS) to confirm the presence of iron.

Figure 6. Protein and RNA levels of iron-related genes in liver and spleen of Pfn2$^{-/-}$ and wt mice. Liver (A) L-ferritin and H-ferritin protein levels measured by Western blotting are reduced in Pfn2$^{-/-}$ mice compared to wt controls, while splenic (D) ferroportin protein levels are increased in Pfn2$^{-/-}$ mice compared to wt controls. Ribosomal protein S6 levels were used for calibration. Graphs represent quantified data normalized to the wt sample (set as 100%). Samples size (n) is indicated. RNA expression of iron-related genes was analyzed by qPCR in liver (C) and spleen (E). mRNA expression was calibrated with *RPL19* and *Tbp* mRNA expression and normalized to wild type mice (set as 100%). Sample size (n) is indicated. Plasma levels of IL6 were measured by Luminex immunoassay (B), data is shown as means ± SEM. The following abbreviations are used: Fth1: H-ferritin; Ftl: L-ferritin; Tfrc: transferrin receptor 1; Slc11a2: divalent metal transporter 1; Slc40a11 (protein: Fpn1): ferroportin; Lcn2: Lipocalin 2; Hamp1: hepcidin; Bmp6: Bone morphogenetic protein 6; IL6: Interleukin 6.

Figure 7. Model for systemic iron distribution and homeostasis in wt versus *Pfn2*$^{-/-}$ mice. Pfn2 KO mice exhibit brain iron accumulation and depletion of liver iron stores with normal hematological parameters. Brain iron overload can be attributed to an increase in transferrin-transferrin receptor endocytosis (Tf-Fe^{3+}-TfR1) due to the lack of Pfn2 that negatively regulates this process. While in wild-type mice erythropoiesis is supported mainly by liver but also splenic iron, in Pfn2$^{-/-}$ mice erythropoiesis is supported exclusively by splenic iron where we have detected a substantial increase in ferroportin (Fpn1) production. In Pfn2$^{-/-}$ mice *hepcidin* (*Hamp1*) production in liver is inappropriately normal despite low iron levels, which should down-regulate *hepcidin* production in order to

increase dietary iron absorption and restore liver iron content. *Hepcidin* inappropriately normal levels in liver of $Pfn2^{-/-}$mice are caused by a mild increase in the release of IL6 pro-inflammatory cytokine that can over-rule opposite inhibitory signals.

Figure 1

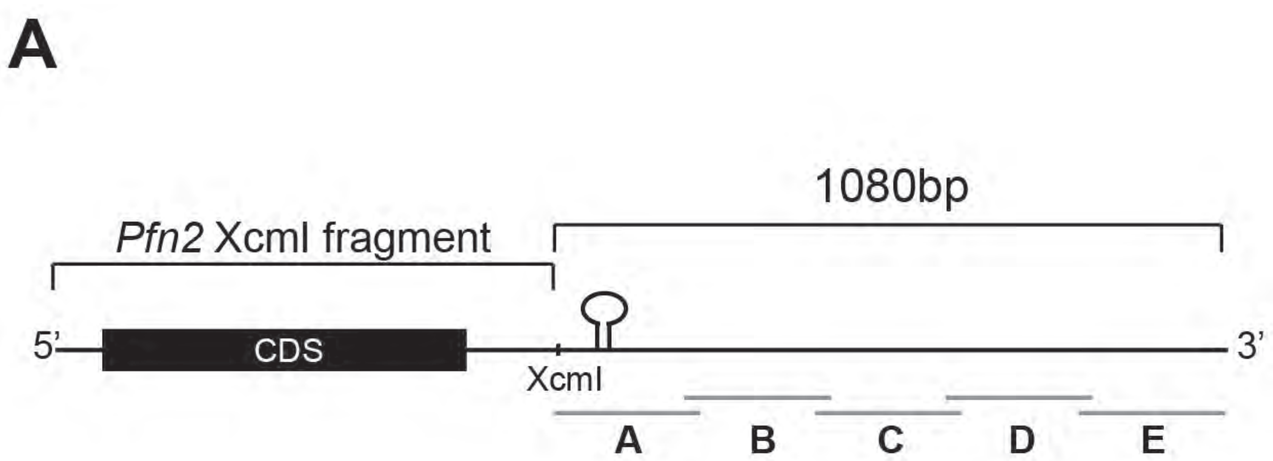

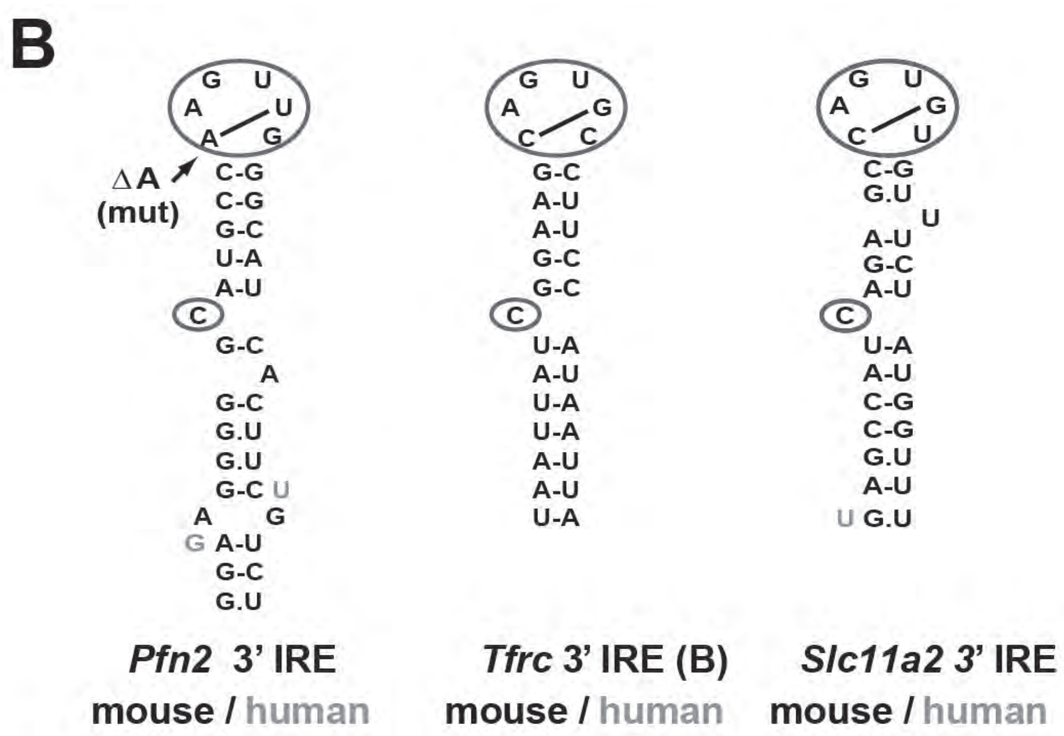

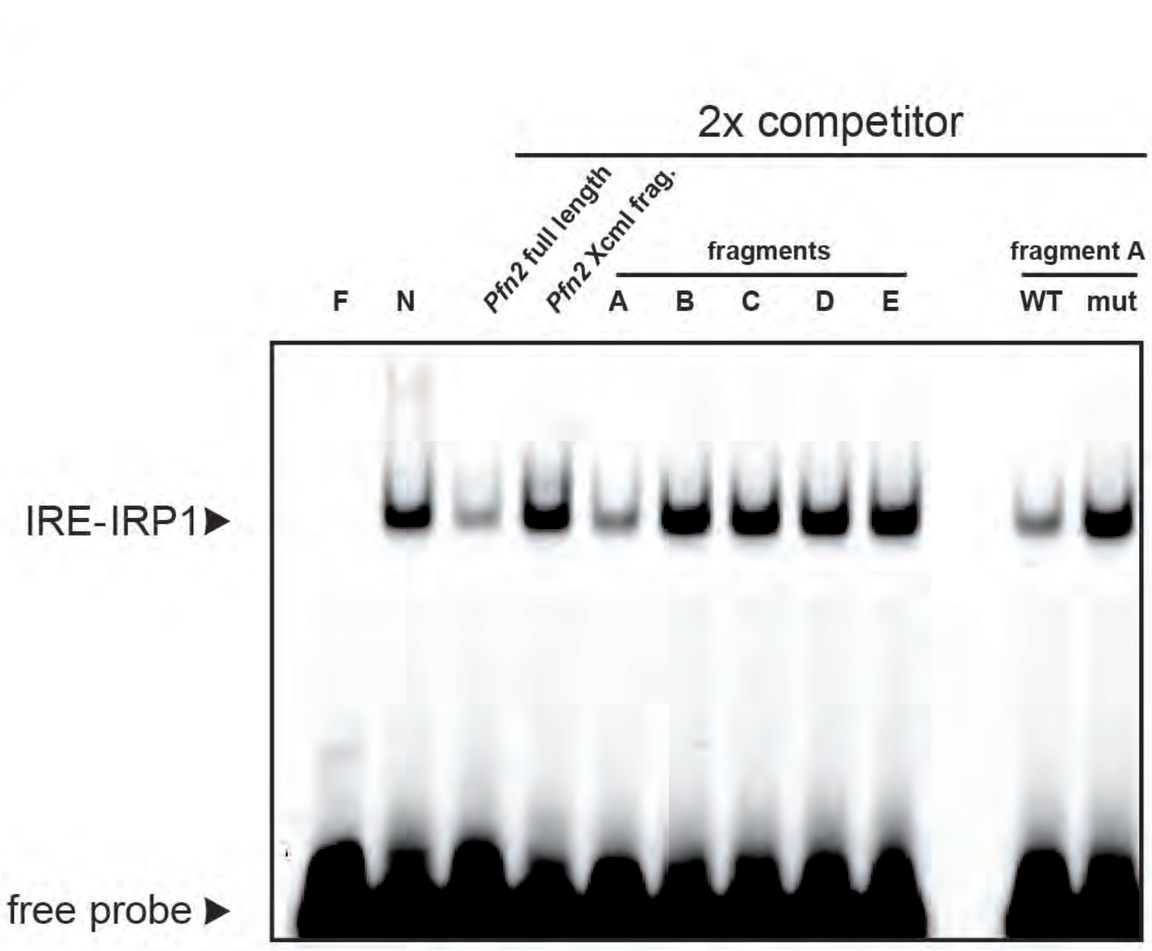

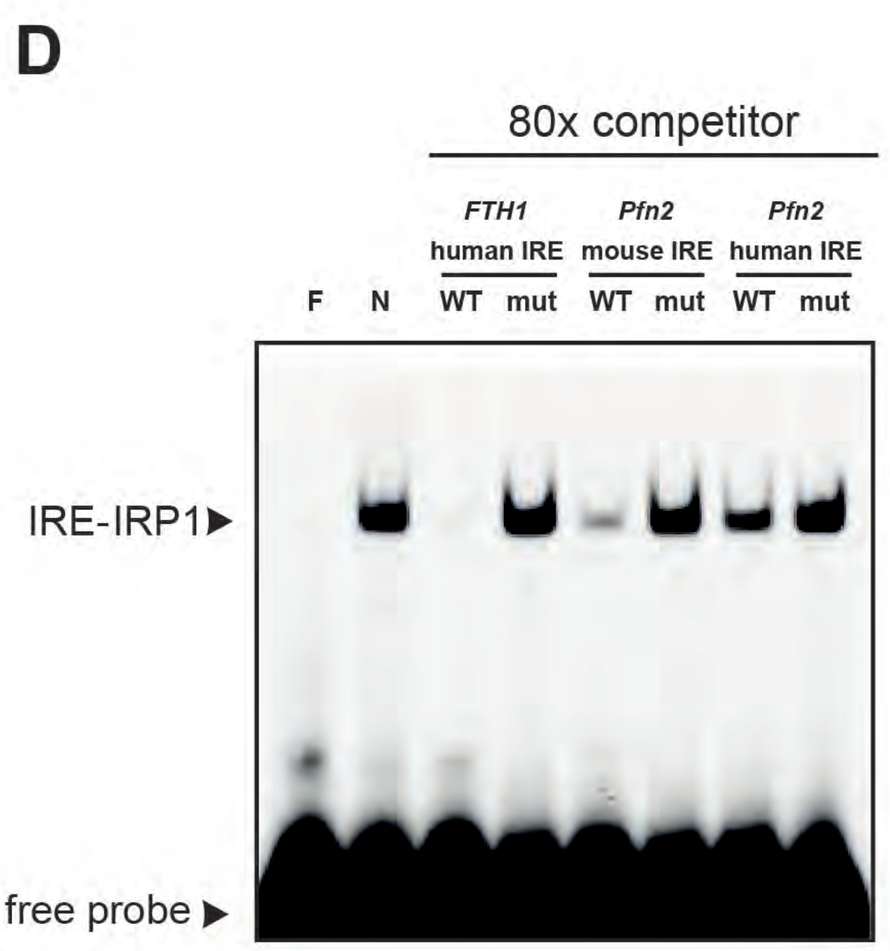

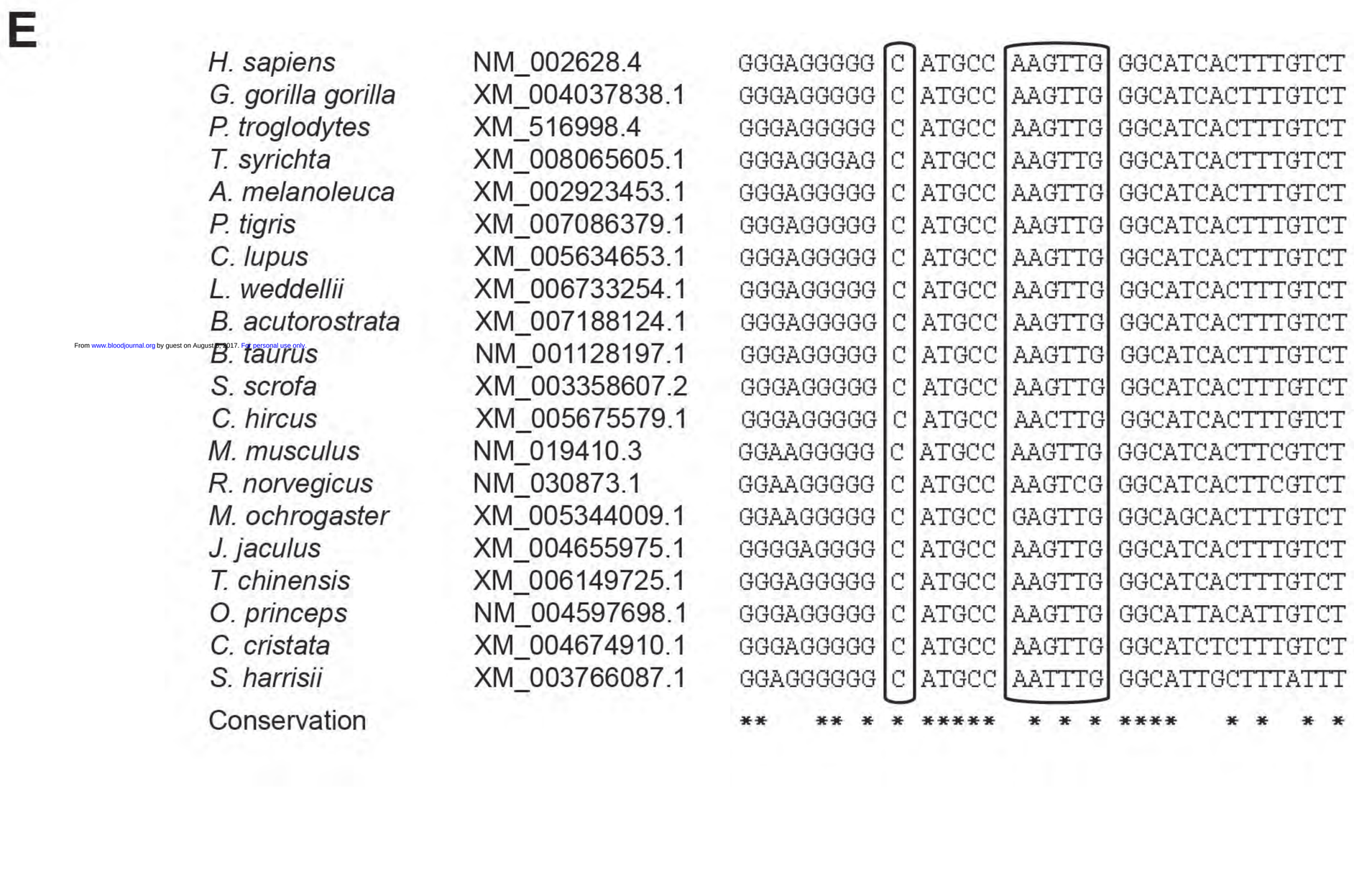

Figure 2

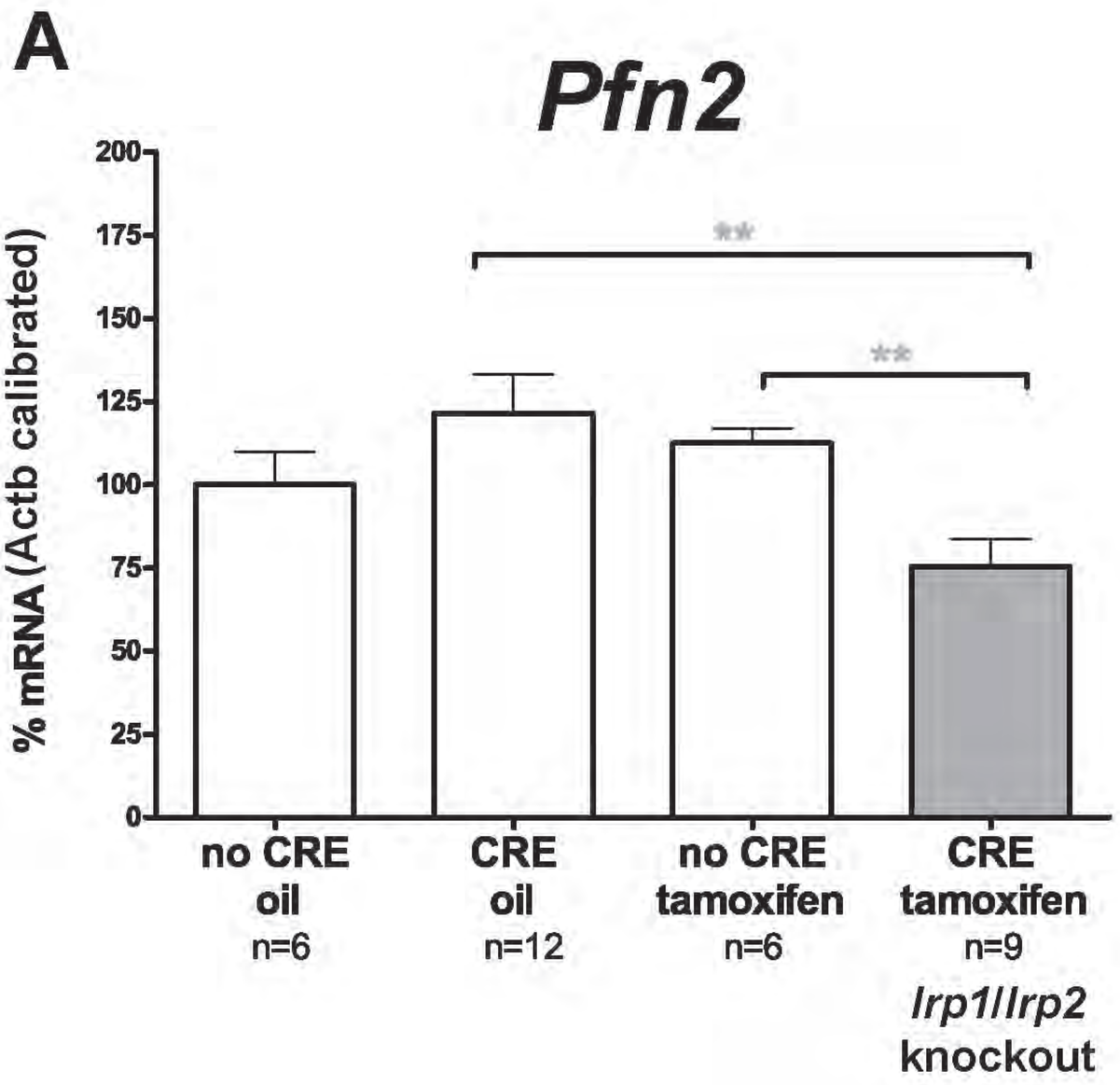

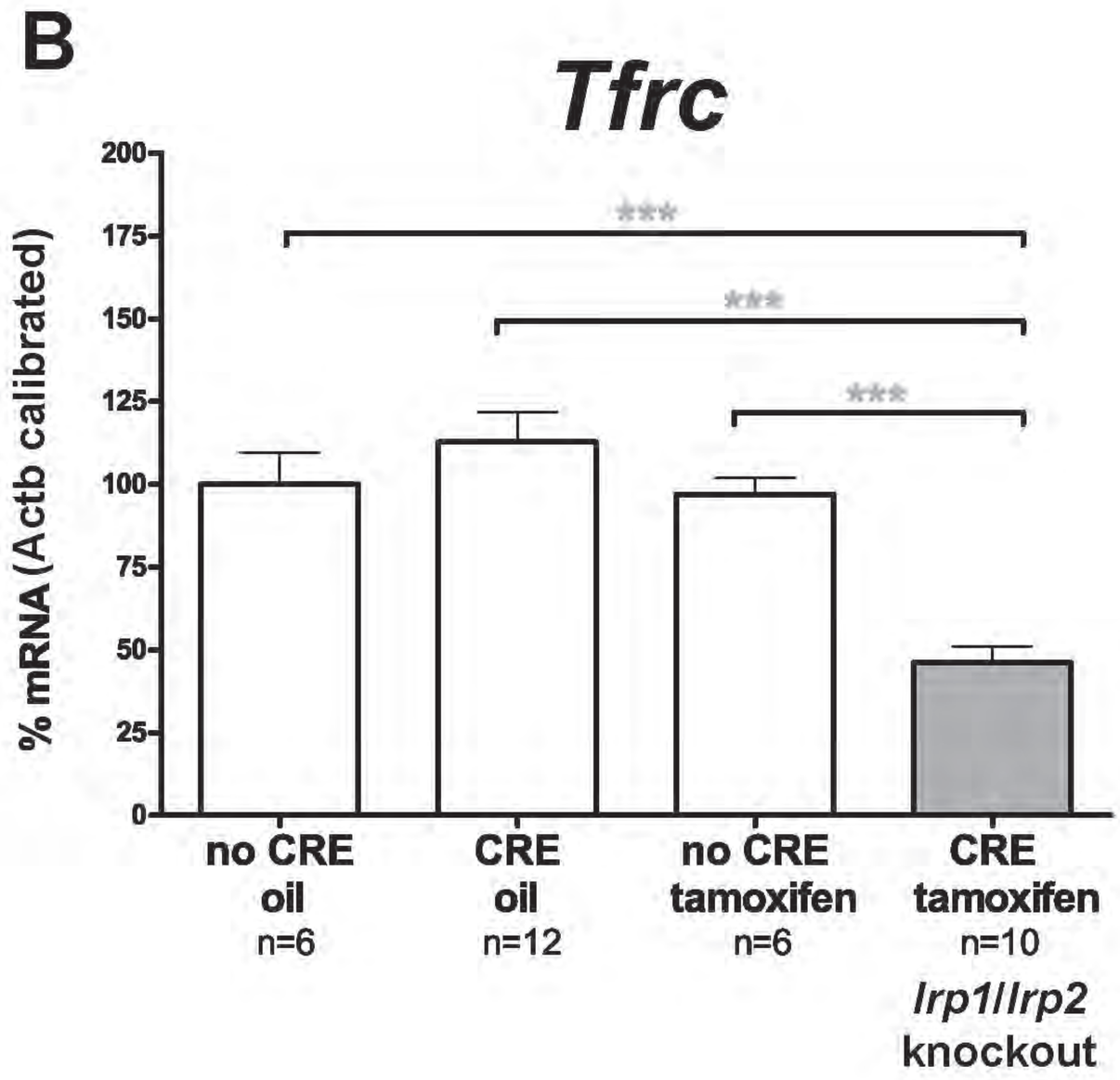

Figure 3

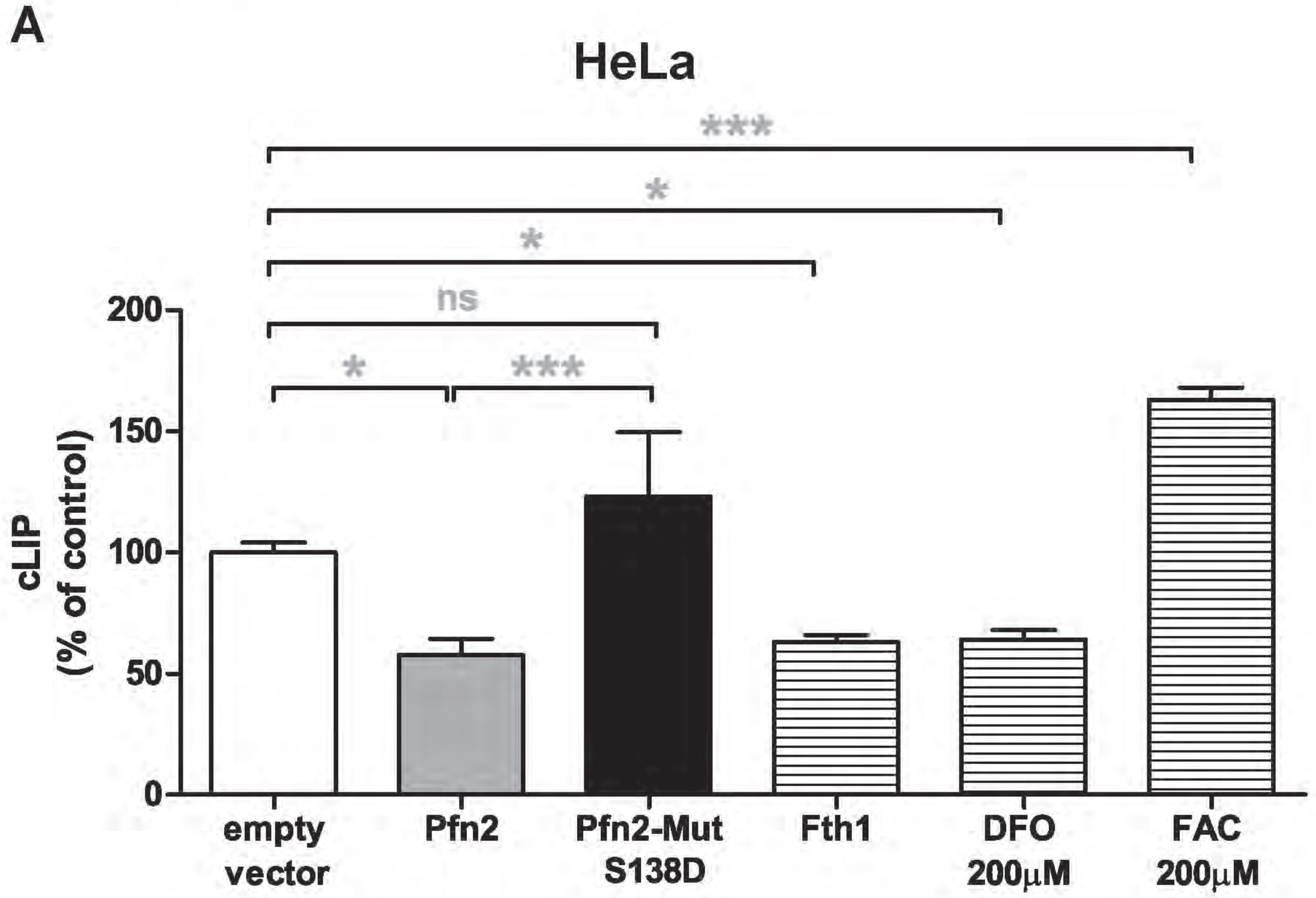

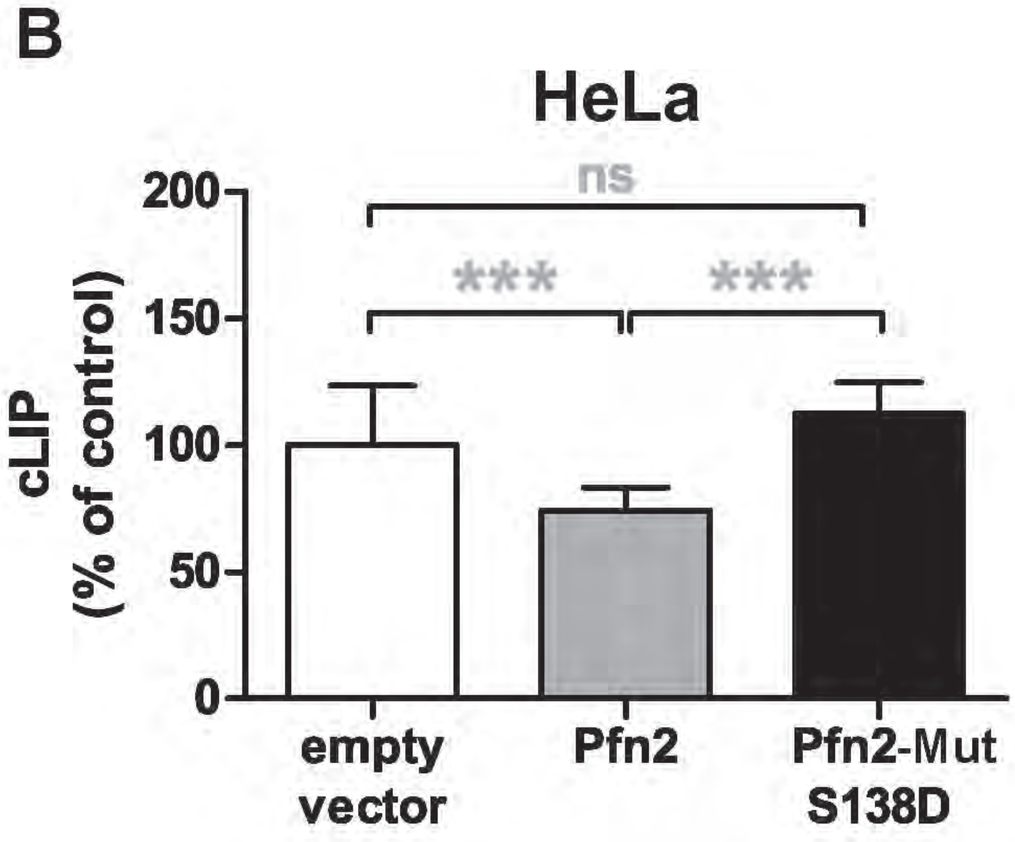

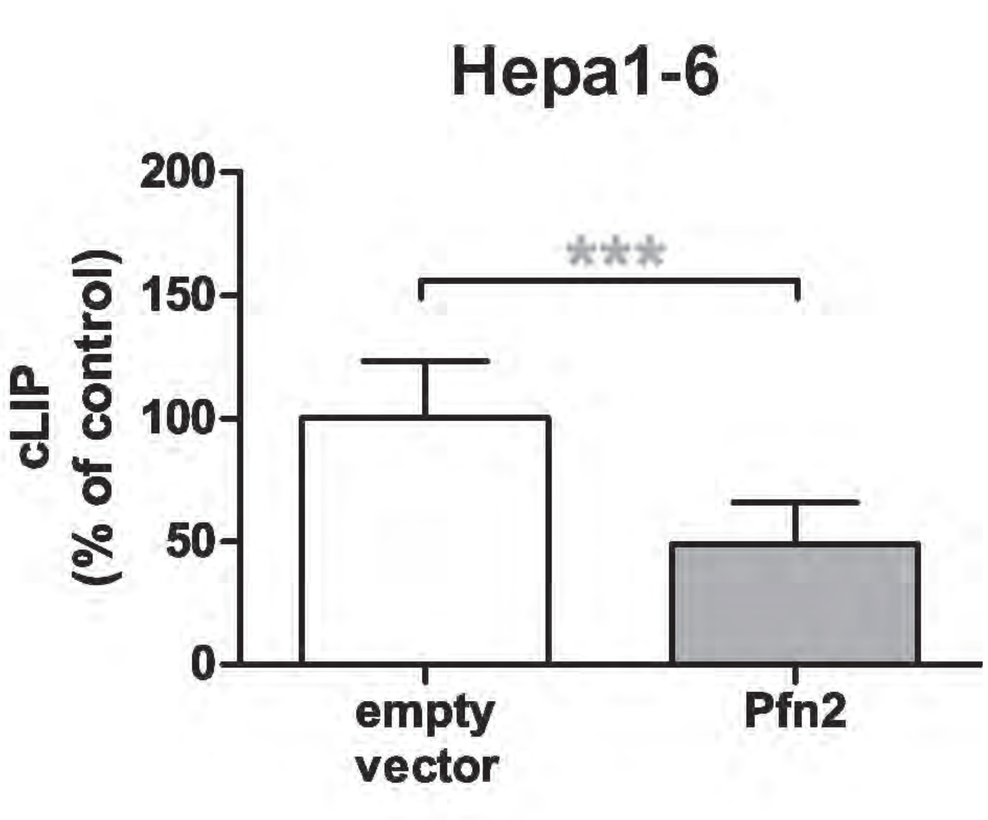

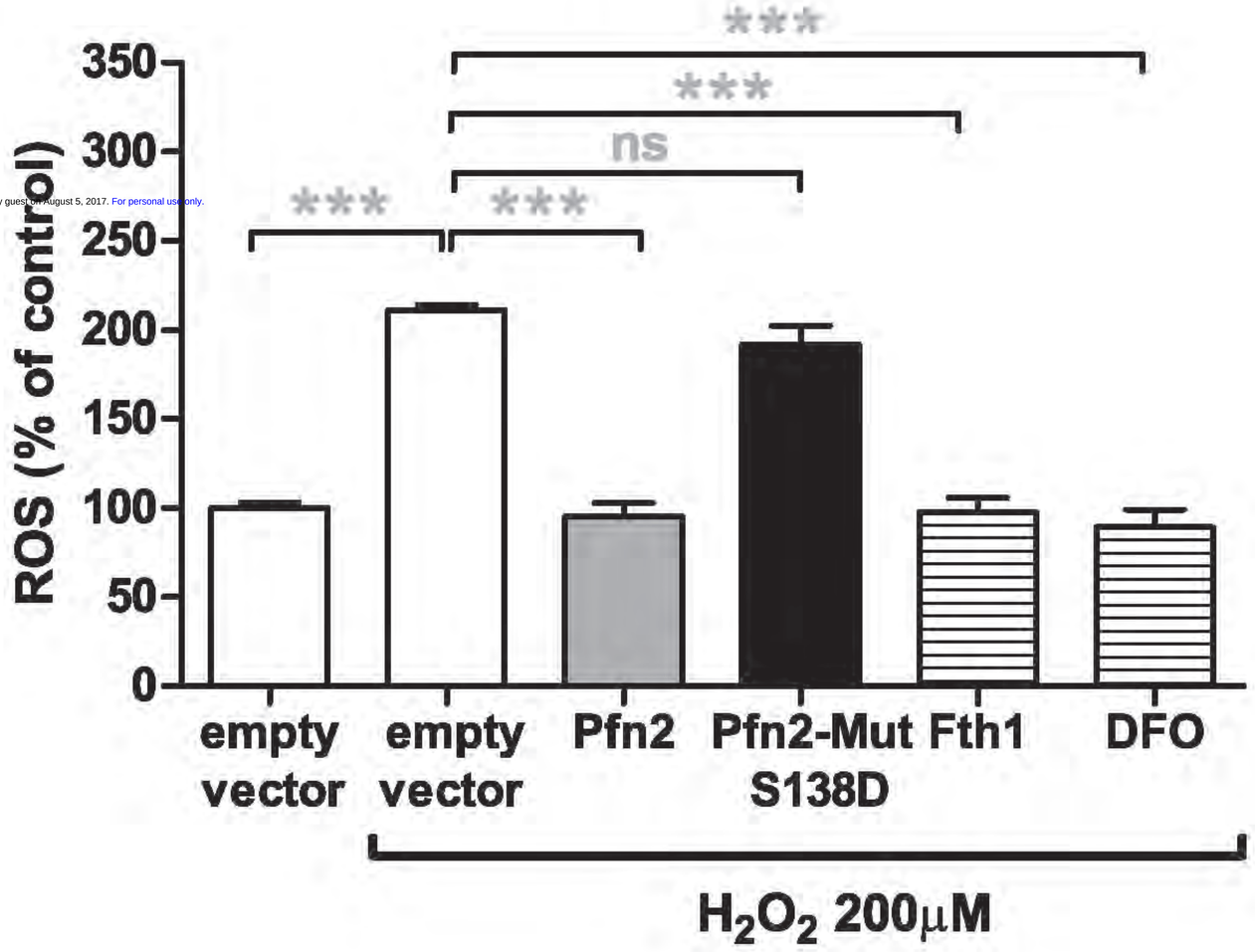

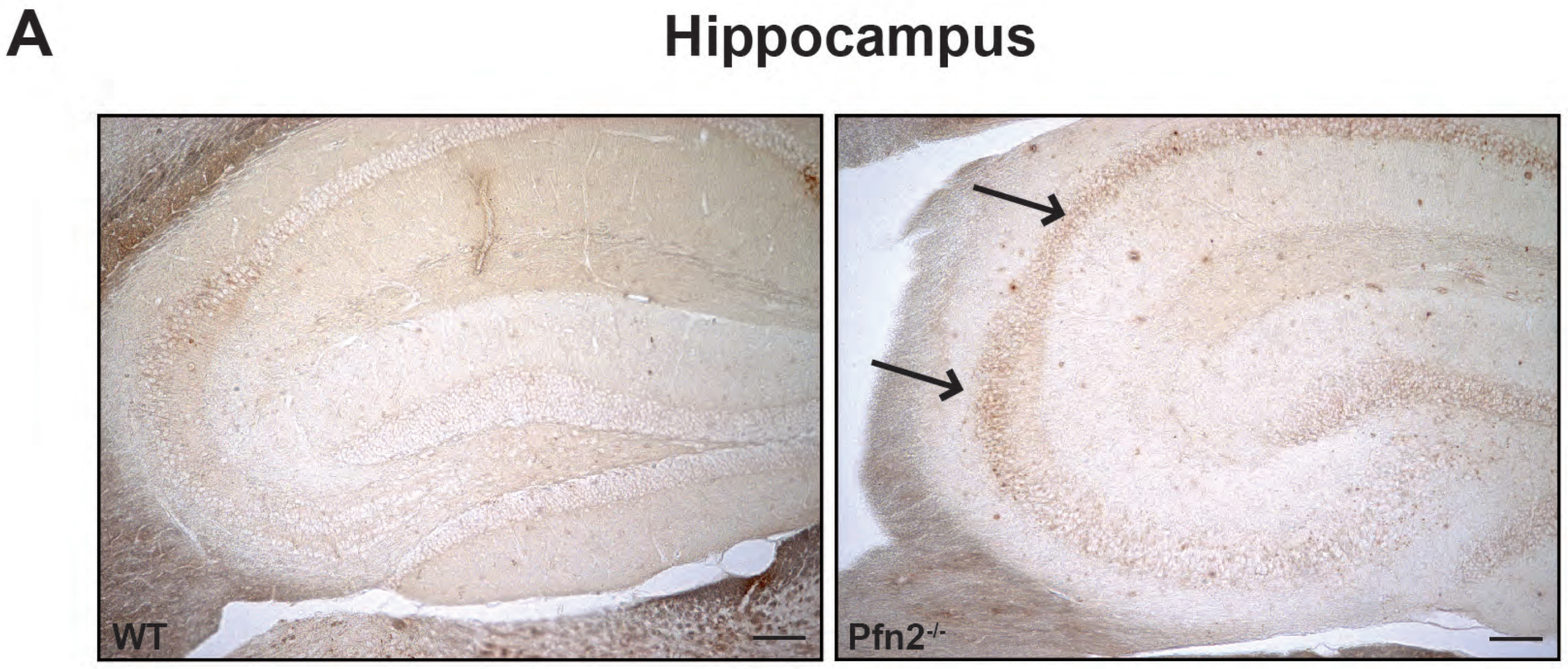

Figure 4

Figure 5

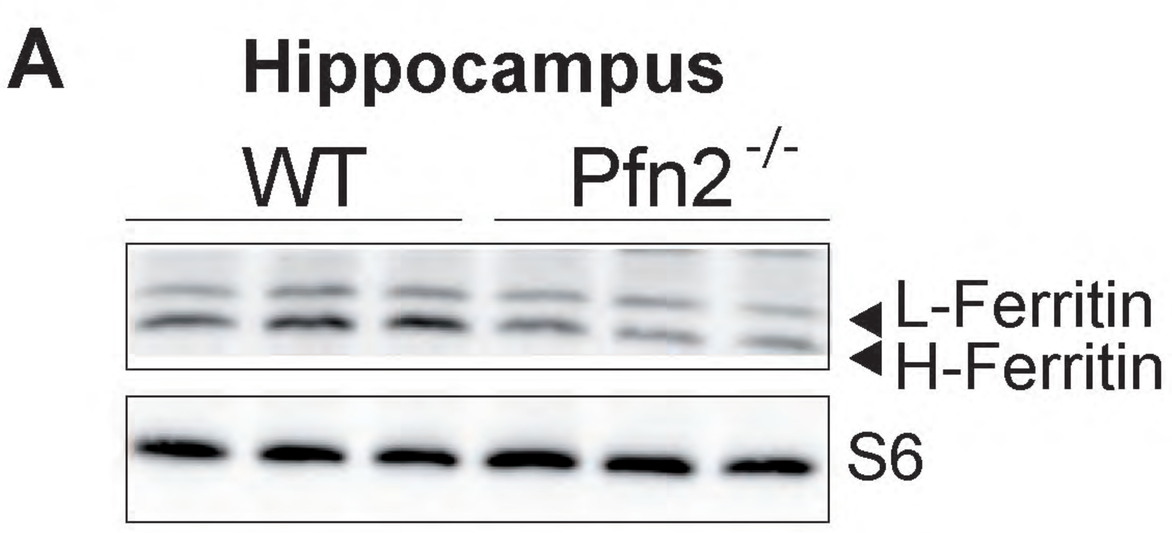

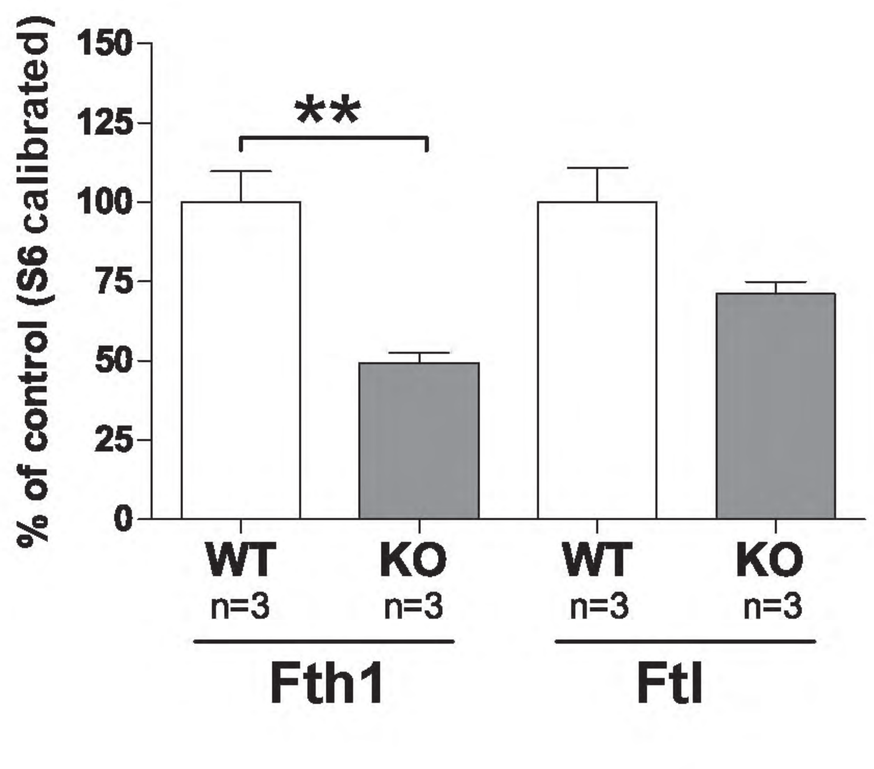

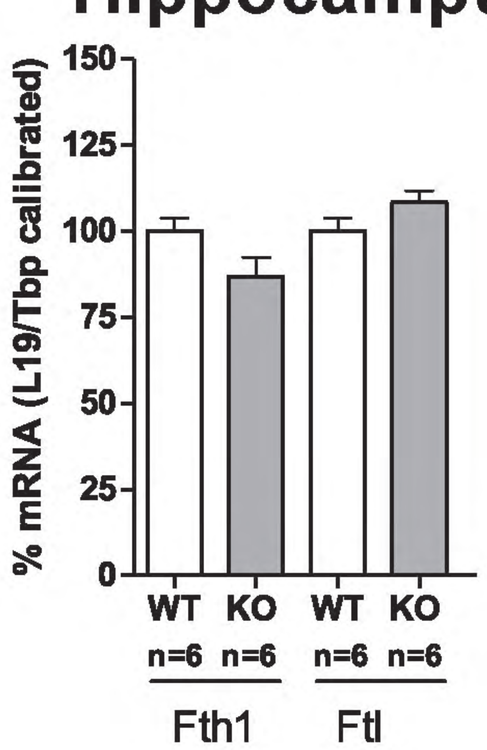

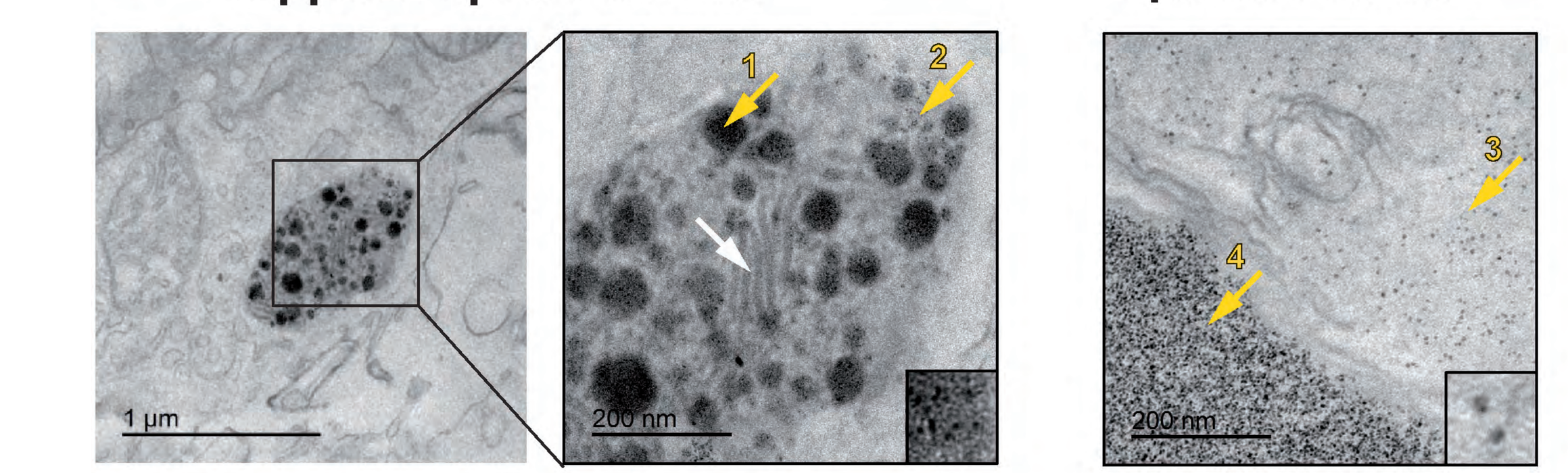

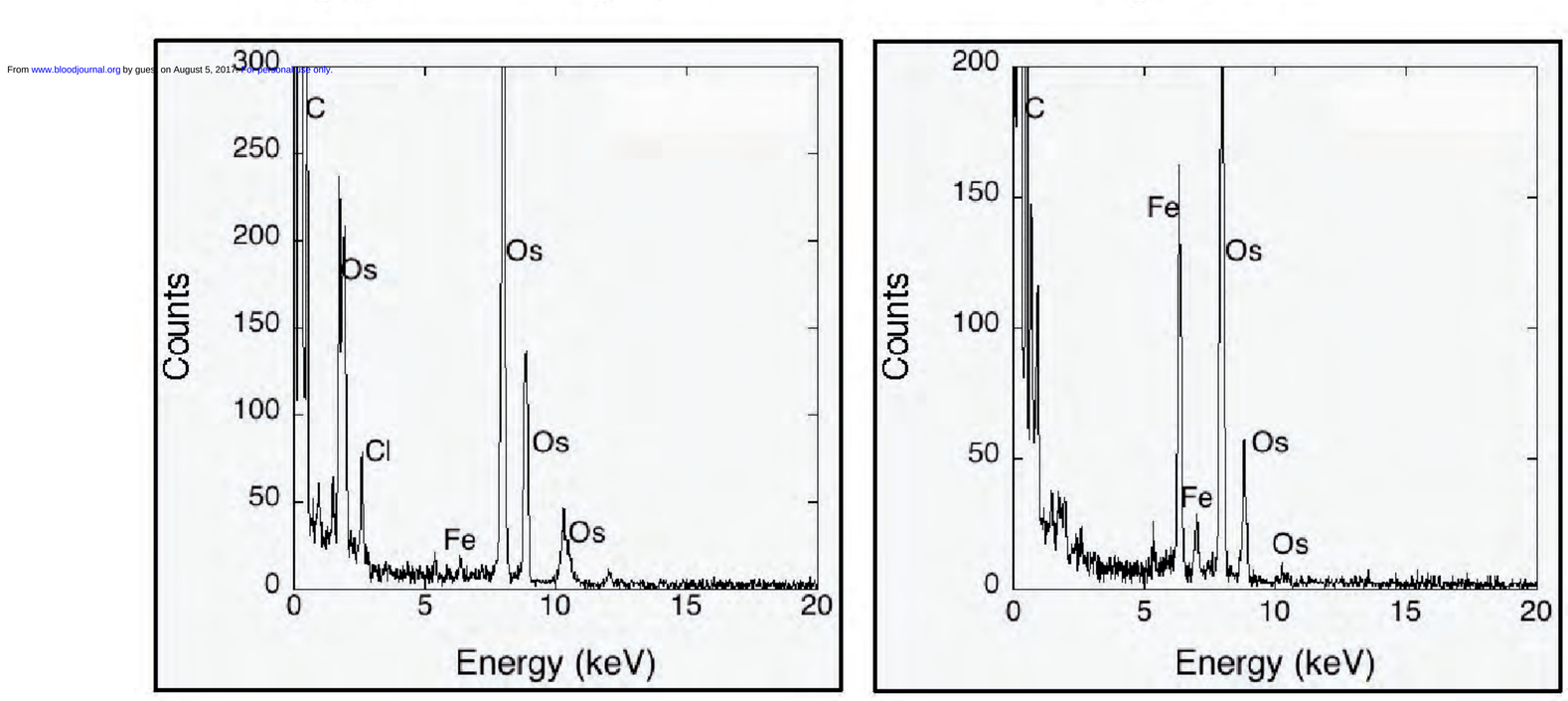

Figure 6

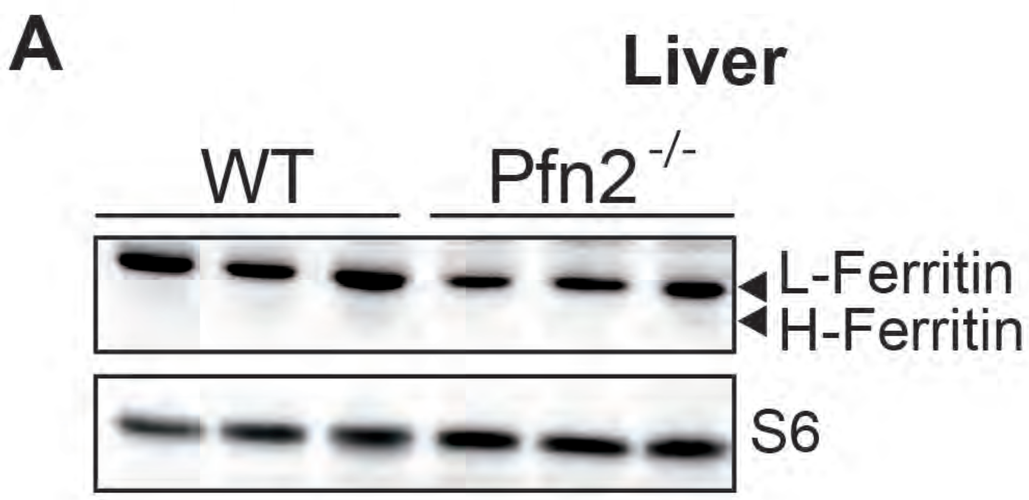

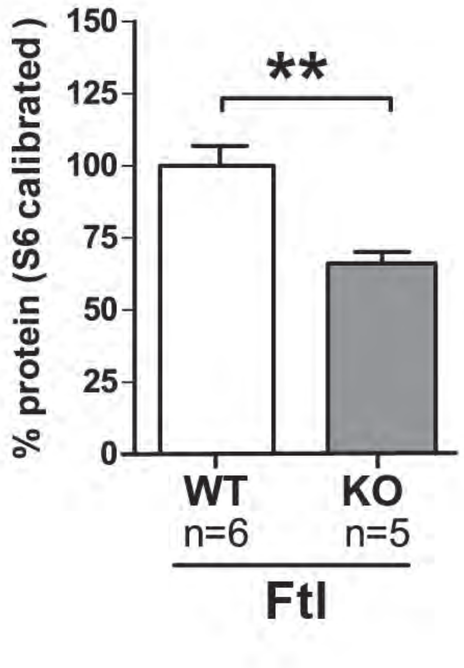

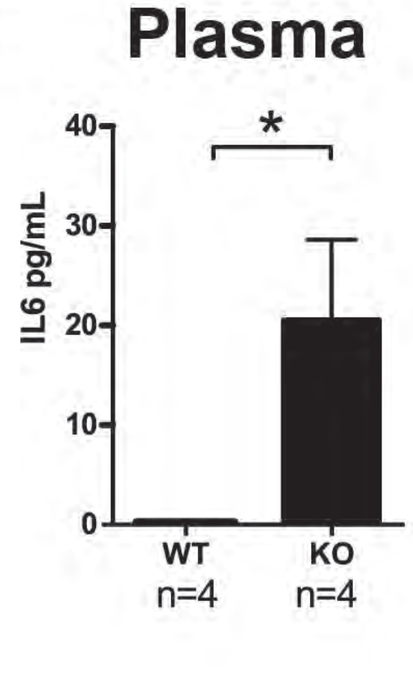

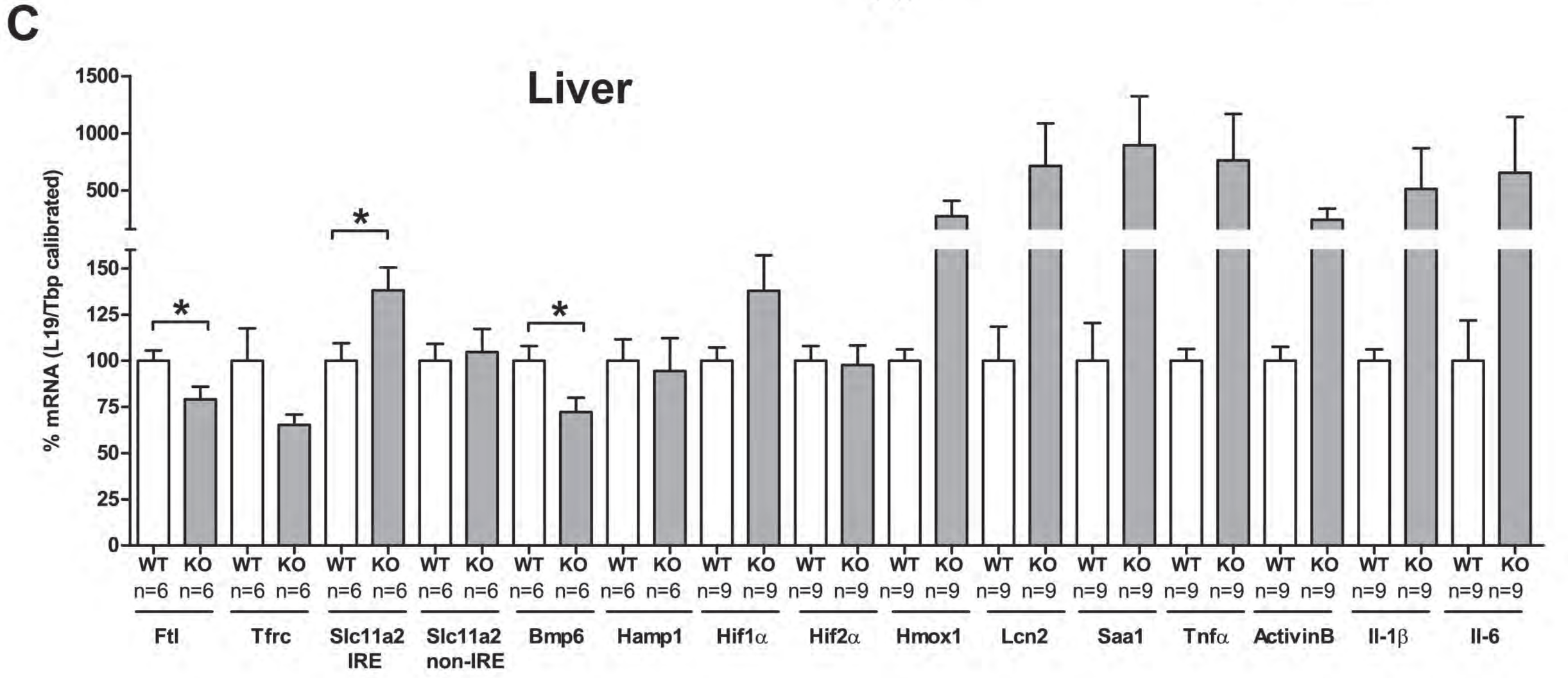

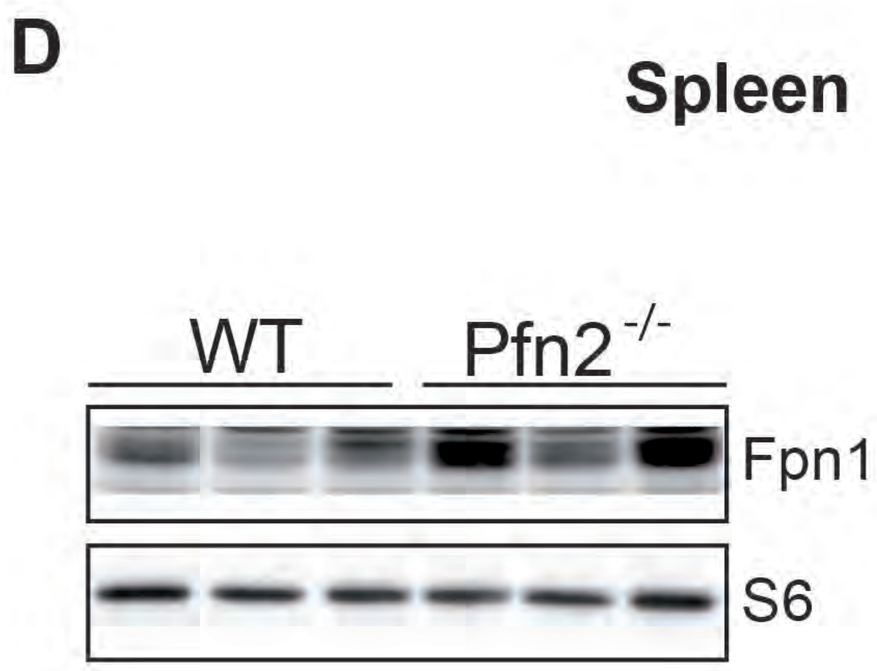

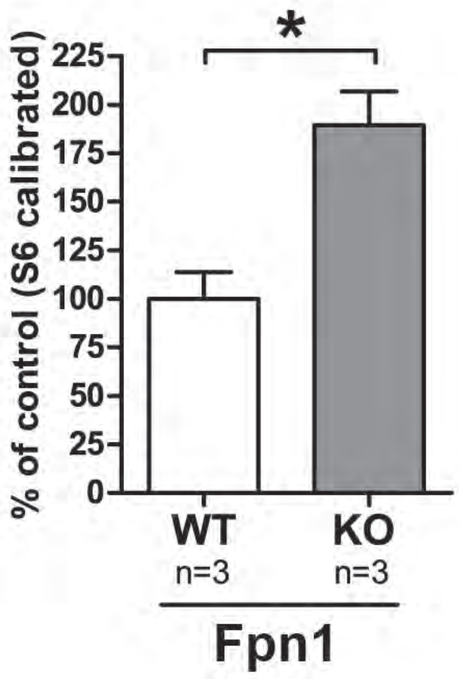

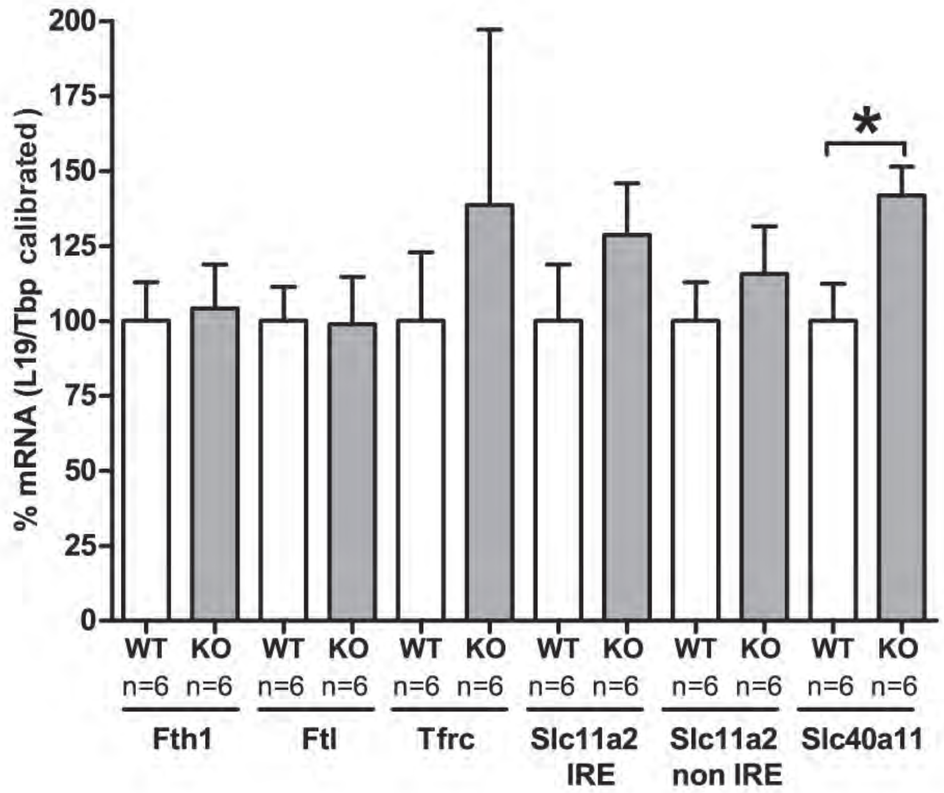

Figure 7

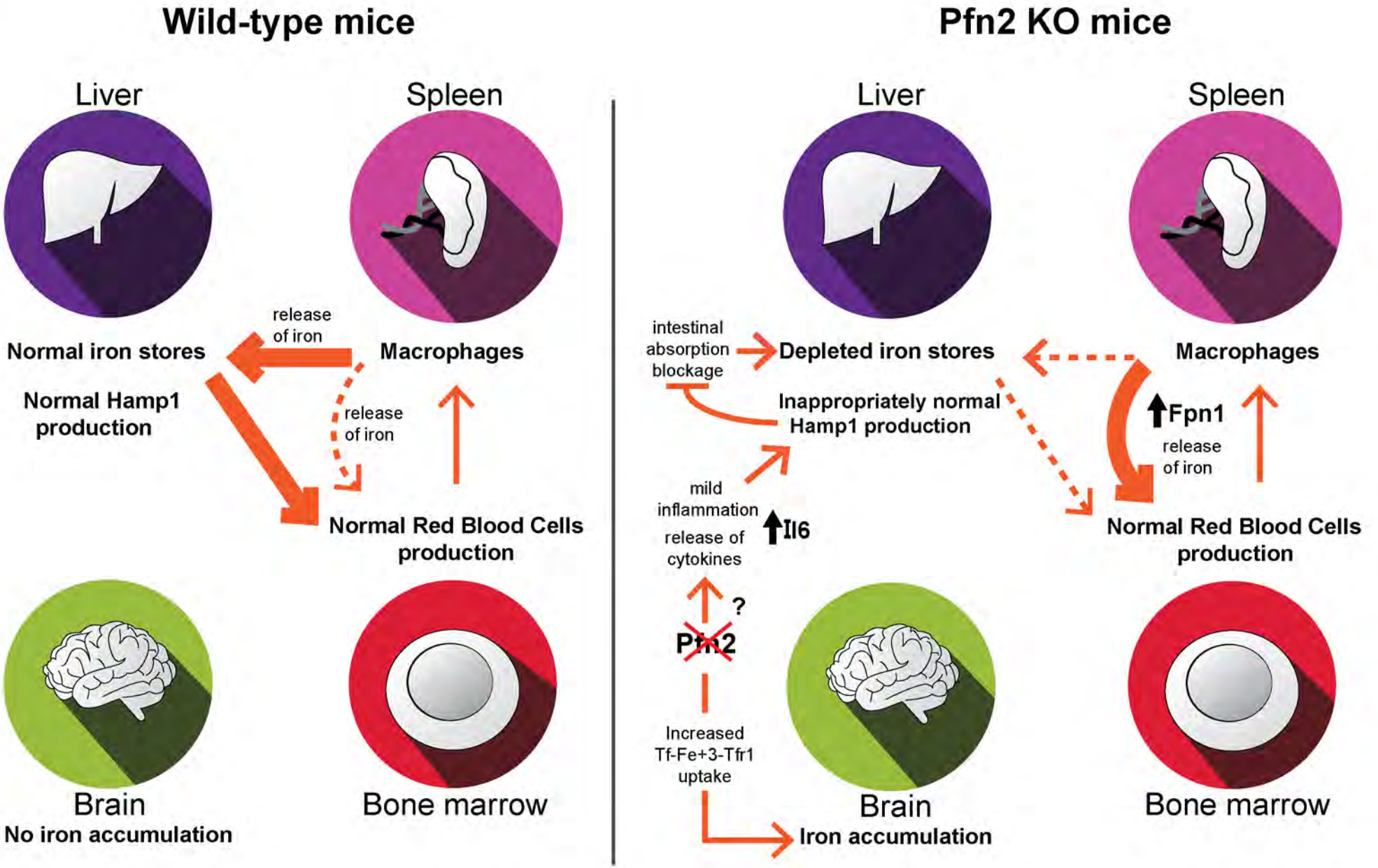
Wild-type mice
Liver
Spleen
release of iron
Normal iron stores
Macrophages
Normal Hamp1 production
release of iron
Normal Red Blood Cells production
Brain
No iron accumulation
Bone marrow
Pfn2 KO mice
Liver
Spleen
intestinal absorption blockage
Depleted iron stores
Macrophages
Inappropriately normal Hamp1 production
Fpn1
release of iron
mild inflammation
release of cytokines
Il6
Normal Red Blood Cells production
?
Pfn2
Increased Tf-Fe+3-Tfr1 uptake
Brain
Iron accumulation
Bone marrow

Prepublished online August 3, 2017;
doi:10.1182/blood-2016-11-754382

The actin binding protein profilin 2 is a novel regulator of iron homeostasis

Sara Luscieti, Bruno Galy, Lucia Gutierrez, Michael Reinke, Jorge Couso, Maya Shvartsman, Antonio Di Pascale, Walter Witke, Matthias W. Hentze, Pietro Pilo Boyl and Mayka Sanchez

Blood (print ISSN 0006-4971, online ISSN 1528-0020), is published weekly by the American Society of Hematology, 2021 L St, NW, Suite 900, Washington DC 20036.